Photochemical Reaction Mechanisms of 2-Nitrobenzyl Compounds: Methyl Ethers and Caged ATP

Yuri V. Il'ichev,[†] Markus A. Schwörer,[‡] and Jakob Wirz*

*Contribution from the Departement Chemie der Universität Basel, Klingelbergstr. 80,
CH-4056 Basel, Switzerland*

Received October 15, 2003; E-mail: J.Wirz@unibas.ch

Abstract: The mechanism of methanol photorelease from 2-nitrobenzyl methyl ether (**1**) and 1-(2-nitrophenyl)ethyl methyl ether (**2**), and of ATP release from adenosine-5′-triphosphate-[P^3-(1-(2-nitrophenyl)-ethyl)] ester ('caged ATP', **3**) was studied in various solvents by laser flash photolysis with UV−vis and IR detection. In addition to the well-known primary *aci*-nitro transients (**A**, $\lambda_{max} \approx 400$ nm), two further intermediates preceding the release of methanol, namely the corresponding 1,3-dihydrobenz[*c*]isoxazol-1-ol derivatives (**B**) and 2-nitrosobenzyl hemiacetals (**C**), were identified. The dependencies of the reaction rates of **A**−**C** on pH and buffer concentrations in aqueous solution were studied in detail. Substantial revision of previously proposed reaction mechanisms for substrate release from 2-nitrobenzyl protecting groups is required: (a) A novel reaction pathway of the *aci*-tautomers **A** prevailing in buffered aqueous solutions, e.g., phosphate buffer with pH 7, was found. (b) The cyclic intermediates **B** were identified for the first time as the products formed by the decay of the *aci*-tautomers **A** in solution. A recently proposed reaction pathway bypassing intermediates **B** (Corrie et al. *J. Am. Chem. Soc.*, **2003**, *125*, 8546−8554) is shown not to be operative. (c) Hemiacetals **C** limit the release rate of both **1** (pH < 8) and **2** (pH < 10). This observation is in contrast to a recent claim for related 2-nitrobenzyl methyl ethers (Corrie et al.). Our findings are important for potential applications of the 2-nitrobenzyl protecting group in the determination of physiological response times to bioagents ('caged compounds').

Introduction

The 2-nitrobenzyl functionality is the most widely used photoremovable protecting group for application in synthesis,[1] photolithography (DNA microarrays),[2] and biochemistry ("caged compounds").[3] Physiological response times to bioagents such as neurotransmitters may be determined, if the release of a signaling molecule following pulsed excitation of the protected precursor is faster than the response time under investigation.[4] The primary photoreaction of 2-nitrobenzyl compounds is intramolecular H-atom transfer affording *aci*-nitro tautomers that are readily detected by their strong absorption around 400 nm. Their decay is often taken to indicate the release rate of the protected agents. However, the subsequent reactions leading to release of the protected leaving groups are not well understood.

Here, we report a study of the model compounds 2-nitrobenzyl methyl ether (**1**) and 1-(2-nitrophenyl)ethyl methyl ether (**2**) by picosecond pump−probe spectroscopy, nanosecond laser flash photolysis (LFP), and time-resolved infrared (TRIR) spectroscopy. Two additional intermediates that are formed from the primary *aci*-nitro photoproducts were identified and the rate of methanol photorelease from nitrobenzyl-protected substrates was found to be orders of magnitude slower than that for the decay of the primary *aci*-nitro transients in aqueous solution at pH ≈ 7. 'Caged ATP',[5] the disodium salt of adenosine-5′-triphosphate-[P^3-(1-(2-nitrophenyl)ethyl)] ester (**3**) was also briefly investigated. A related study on derivatives of **1** and **2** was published[6] after the completion of our work,[7] and will be referred to in the discussion. A well-known problem with the use of 2-nitrobenzyl and 2-nitrophenethyl protecting groups in biological preparations is that the release of the desired bioactive compounds is accompanied by the formation of 2-nitrosobenzaldehyde or 2-nitrosoacetophenone, respectively, which may inactivate the biological preparations or give rise to further, undesired but harmful photoreactions. Secondary photoreactions of the nitroso products were not investigated here. In a previous publication, we have reinvestigated the largely reversible

† Present address: Wichita State University, Department of Chemistry, 1845 Fairmount St., Wichita, KS 67260-0051.
‡ Present address: MDL Information Systems GmbH, Theodor-Heuss-Allee 108, D-60486 Frankfurt/Main, Germany.

(1) Pillai, V. N. R. *Synthesis* **1980**, 1−26. Greene, T. W.; Wuts, P. G. M. *Protective Groups in Organic Synthesis*, 3rd ed.; Wiley-Interscience: New York, 1999.
(2) Chee, M.; Yang. R.; Hubbell, E.; Berno, A.; Huang, X. C.; Stern, D.; Winkler, J.; Lockhart, D. J.; Morris, M. S.; Fodor, S. P. A. *Science* **1996**, *274*, 610−614. Pirrung, M. C. *Chem. Rev.* **1997**, *97*, 473−488. Pirrung, M. C. *Angew. Chem., Int. Ed.* **2002**, *41*, 1276−1289.
(3) Pelliccioli, A. P.; Wirz, J. *Photochem. Photobiol. Sci.* **2002**, *1*, 441−458.
(4) Breitinger, H.-G. A.; Wieboldt, R.; Ramesh, D.; Carpenter, B. K.; Hess, G. P. *Biochemistry* **2000**, *39*, 5500−5508. Givens, R. S.; Weber, J. F. W.; Conrad, P. G.; Orosz, G.; Donahue, S. L.; Thayer, S. A. *J. Am. Chem. Soc.* **2000**, *123*, 2687−2697. Pollock, J.; Crawford, J. H.; Wootton, J. F.; Corrie, J. E. T.; Scott, R. H. *Neurosci. Lett.* **2003**, *338*, 143−146.

(5) Kaplan, J. H.; Forbush, B.; Hoffman, J. F. *Biochemistry* **1978**, *17*, 1929−1935.
(6) Corrie, J. E. T.; Barth, A.; Munasinghe, V. R. N.; Trentham, D. R.; Hutter, M. C. *J. Am. Chem. Soc.* **2003**, *125*, 8546−8554.
(7) Schwörer, M. 'Mechanismen der lichtinduzierten Freisetzung von Abgangsgruppen aus 2-Nitrobenzylverbindungen', Ph.D. thesis, University of Basel, 2002, and ref 3.

Scheme 1. Phototautomerization of 2-Nitrotoluene
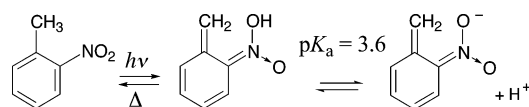
phototautomerization of parent 2-nitrotoluene (Scheme 1) to identify the elementary steps of the thermal back reaction in aqueous solution as a benchmark.[8] In a forthcoming paper, we will discuss the photoreactions of 2-nitrobenzyl alcohols.[9]
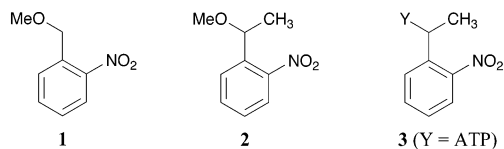
Experimental Section

Methods. Reaction quantum yields were determined by spectrophotometric monitoring of the absorbance changes. A medium-pressure mercury lamp equipped with a 365-nm band-pass filter was used as a light source. Actinometry was done with a solution of azobenzene in methanol.[10]

The nanosecond kinetic and spectroscopic laser flash photolysis setup was of standard design. An excimer laser operated mostly on KrF (248 nm), but also on XeCl (308 nm) or XeF (351 nm), was used as an excitation source with a pulse duration of about 25 ns and pulse energies of <200 mJ. Neither degassing nor changing the excitation wavelength had a noticeable effect on the transient intermediates. Therefore, most measurements were done with aerated solutions. All kinetic measurements with aqueous solutions were done at ambient temperatures (23 $\pm$ 2 °C) and at ionic strength $I = 0.1$ M, which was adjusted by addition of NaClO$_4$. Consequently, all the equilibrium constants so determined are molar concentration quotients, K_c, for $I = 0.1$ M. Transients with lifetimes exceeding 1 ms were measured on a conventional kinetic flash apparatus with a thermostated sample cell (25.0 $\pm$ 0.1 °C) using a discharge flashlamp ($\leq$1000 J) for excitation.

The picosecond pump–probe setup has been described.[11] Solutions with an absorbance of 0.5 (1 mm path length) were circulated in a flow system, pumped at 248 nm (4 mJ, 0.7 ps half-width, 10 Hz) and probed by a delayed continuum pulse (310–700 nm) of the same duration. Transient absorption spectra were recorded at ca. 50 different time delays ranging from 2 ps to 1.8 ns relative to the excitation pulse and subjected to factor analysis.

The step-scan instrument was built by the design of Rödig and Siebert[12] using a Bruker IFS 66v/s Fourier transform infrared spectrophotometer equipped with a globar IR source, a KBr beam splitter, a nitrogen-cooled MCT detector (KV100-1-B-7/190) and an external DC-coupled preamplifier from Kolmar Inc. (KA020-E6/MU/B). A Quantel Brilliant W Nd:YAG laser (266 or 355 nm, pulse width 6 ns, pulse energy $\leq$5 mJ, pulse frequency 10 Hz) was used for excitation and a Germanium filter was positioned behind the cell to absorb the laser beam. The spectral window was restricted to 1000–2000 cm^{-1} by using a cut-on/cutoff filter combination from LOT Oriel. Solutions with an optical density of 0.4 were pumped through the sample cell (CaF$_2$ windows, 100-μm path length) to avoid re-irradiation of transient intermediates and photoproducts. The Fourier transformed interferograms (128 accumulations, spectral resolution 8 cm^{-1}, 3-term Black-

man-Harris apodization function, Mertz phase correction, zero-filling factor of 4) gave a set of IR difference spectra (post-flash minus pre-flash absorbance) at varying delay times, which was subjected to factor analysis. A few significant factors (usually 2) were generally sufficient to reproduce the time evolution of the spectra within experimental accuracy. This procedure resulted in a substantial reduction of noise. Mono- or biexponential decay functions, as required, were fitted to the reduced set of spectra so obtained. The temperature in the sample compartment was 30 °C during operation. Fast-scan spectra for transients with a lifetime exceeding 100 ms were recorded on standing solutions of 100–500 μm path length after exposing the sample to one or several laser flashes.

Materials. Doubly distilled water was used to prepare aqueous solutions. All other solvents were of spectroscopic grade and were used as received. The absorbance of the neat solvents at 248 nm was less than 0.01 at 1-cm path length. Ethers **1** and **2** were synthesized by methylation of the corresponding alcohols with dimethyl sulfate using phase transfer catalysis.[13–15] Caged ATP (**3**) was purchased from Molecular Probes.

2-Nitrosobenzaldehyde (4):[16] A solution of anthranil (3 g, 25.2 mmol) in aqueous HCl (37 g, 23%) was cooled to −20 °C. Powdered NaNO$_2$ (1.75 g, 25.3 mmol) was added in small portions. The resulting yellow-brown slurry was stirred for 20 min at −20 °C and filtered. The solid was washed with cold aqueous HCl (6 mL, 23%) and water, and redissolved in 10 mL of 2 M NaOH at 0 °C. Insoluble material was removed by filtration and the filtrate was added to a cold solution of 4 mL of concentrated H$_2$SO$_4$ in 75 mL water with vigorous stirring. The resulting brown suspension was stirred at 0 °C for 3 h and filtered. The brown solid was washed with 5 mL of aqueous Na$_2$CO$_3$ (5%), copiously with cold water, and dissolved in CHCl$_3$ (20 mL). Addition of 10 mL petrol ether, bp 60–70 °C, precipitated brown flakes, which were removed by filtration. The green filtrate was shaken with 2% aqueous NaHCO$_3$, washed, evaporated to 5 mL and slowly cooled to −40 °C. 2-Nitrosobenzaldehyde (0.35 g, 2.52 mmol, 10.3% yield) crystallized as bushy needles, mp 110 (113–113.5)[16] °C. ^{1}H NMR (300 MHz, CDCl$_3$/TMS): δ = 6.44 (dd, J_1 = 8, J_2 = 0.8 Hz, 1H), 7.68 (dt, J_1 = 8, J_2 = 1.3 Hz, 1H), 7.91 (dt, J_1 = 8, J_2 = 0.8 Hz, 1H), 8.21 (dd, J_1 = 8, J_2 = 1.3 Hz, 1H), 12.1 (s, 1H, CHO). ^{13}C NMR (75 MHz, CDCl$_3$): δ = 193.3, 162.0, 136.5, 134.0, 132.7, 127.7, 106.5 ppm. MS (EI) m/e (relative intensity): 50 (44), 51 (98), 52 (34), 62 (6), 63 (18), 64 (28), 74 (22), 75 (14), 76 (27), 77 (100), 78 (9), 79 (43), 91 (50), 90 (8), 104 (3), 135 (61). UV/Vis (H$_2$O, 2%THF), λ_{max}/nm (log [ϵ/M^{-1} cm^{-1}]) 238 (4.05), 287 (3.78 $\pm$ 0.02), 310 (3.73 $\pm$ 0.03), 750 (1.34 $\pm$ 0.04).

Calculations. Density Functional Theory (DFT) calculations were performed with the GAUSSIAN 98[17] package of programs. We used the B3LYP hybrid functional, which combines Becke's three-parameter exchange functional[18] with the Lee–Yang–Parr[19] correlation functional in a slightly modified form.[20] Geometries were optimized using the B3LYP functional with the 6-31G(d) and 6-31+G(d) basis sets for

(8) Schwörer, M.; Wirz, J. *Helv. Chim. Acta* **2001**, *84*, 1441−1458.
(9) Il'ichev, Y. V.; Kombarova, S. V.; Mac, M.; Schwörer, M.; Wirz, J. in preparation.
(10) Gauglitz, G.; Hubig, S. *Z. Phys. Chem., N. F.* **1984**, *139*, 237−246. Gauglitz, G.; Hubig, S. *J. Photochem.* **1985**, *30*, 121−125. Persy, G.; Wirz, J. *EPA Newslett.* **1987**, *29*, 45−46.
(11) Hasler, E.; Hörmann, A.; Persy, G.; Platsch, H.; Wirz, J. *J. Am. Chem. Soc.* **1993**, *115*, 5400−5409.
(12) Rödig, C.; Siebert F. *Appl. Spectrosc.* **1999**, *55*, 893−901.

(13) Seebach, D.; Kalinowski, H.-O.; Bastani, B.; Crass, G.; Daum, H.; Dörr, H.; DuPreez, N. P.; Ehrig, V.; Langer, W.; Nüssler, C.; Oei, H.-A.; Schmidt, M. *Helv. Chim. Acta* **1977**, *60*, 301−325.
(14) Merz, A. *Angew. Chem.* **1973**, *85*, 868−869.
(15) Gonzalez, M. A.; Meyers, A. I. *Tetrahedron Lett.* **1989**, *30*, 47−55.
(16) Bamberger, E.; Fodor, A. *Ber. Dtsch. Chem. Ges.* **1910**, *43*, 3321−3335.
(17) Frisch, M. J.; Trucks, G. W.; Schlegel, H. B.; Scuseria, G. E.; Robb, M. A.; Cheeseman, J. R.; Zakrzewski, V. G.; Montgomery, J. A., Jr.; Stratmann, R. E.; Burant, J. C.; Dapprich, S.; Millam, J. M.; Daniels, A. D.; Kudin, K. N.; Strain, M. C.; Farkas, O.; Tomasi, J.; Barone, V.; Cossi, M.; Cammi, R.; Mennucci, B.; Pomelli, C.; Adamo, C.; Clifford, S.; Ochterski, J.; Petersson, G. A.; Ayala, P. Y.; Cui, Q.; Morokuma, K.; Rega, N.; Salvador, P.; Dannenberg, J. J.; Malick, D. K.; Rabuck, A. D.; Raghavachari, K.; Foresman, J. B.; Cioslowski, J.; Ortiz, J. V.; Baboul, A. G.; Stefanov, B. B.; Liu, G.; Liashenko, A.; Piskorz, P.; Komaromi, I.; Gomperts, R.; Martin, R. L.; Fox, D. J.; Keith, T.; Al-Laham, M. A.; Peng, C. Y.; Nanayakkara, A.; Challacombe, M.; Gill, P. M. W.; Johnson, B.; Chen, W.; Wong, M. W.; Andres, J. L.; Gonzalez, C.; Head-Gordon, M.; Replogle, E. S.; Pople, J. A. Gaussian 98, Revision A.11, Gaussian, Inc., Pittsburgh, PA, 2002.
(18) Becke, A. D. *J. Chem. Phys.* **1993**, *98*, 5648−5652.
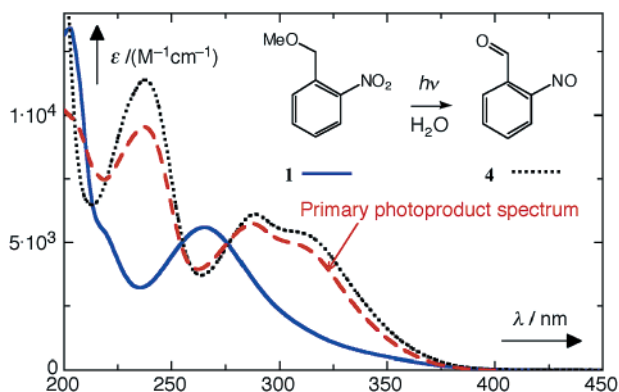(19) Lee, C.; Yang, W.; Parr, R. G. *Phys. Rev. B* **1988**, *37*, 785−797.

Figure 1. Absorption spectra of 2-nitrobenzyl methyl ether (**1**, —), 2-nitrosobenzaldehyde (**4**, ····) and of the primary photoproduct of **1** (- -) in 1×10^{-3} M aqueous $HClO_4$ as determined by EFA.

neutral and anionic species, respectively. B3LYP/6-311+G(2d,p) single-point energies include zero-point vibrational corrections that were scaled with a factor of 0.9806.[21] This level of theory gave satisfactory results in a related study of 2-nitrotoluene.[22] Calculated vibrational frequencies were scaled with a factor of 0.9613 for comparison with IR spectra.[21] Self-consistent reaction field (SCRF) calculations with the polarized continuum model (PCM) of Tomasi and co-workers[23] were utilized to estimate solvent effects. The scaling factor for solvent accessible surfaces and the initial number of tesserae on the surface of each sphere were set to the default values of 1.2 and 60, respectively. Electronic excitation energies were calculated using the random phase approximation for a time-dependent DFT calculation[24] with the B3LYP/6-311+G-(2d,p) basis set.

Results

Photoproducts and Quantum Yields. Irradiation of the methyl ethers **1** and **2** at 254 nm (low-pressure mercury arc) in acetonitrile or in aqueous solution at pH 3−6 generates 2-nitrosobenzaldehyde (**4**) and 2-nitrosoacetophenone (**5**), respectively. The reaction produces strong absorption in the range of 280−350 nm as well as very weak absorption at 750 nm. Due to secondary photolysis of the photoproduct **4**, 2-nitrobenzyl methyl ether (**1**) could not be converted quantitatively. A series of UV spectra obtained by monitoring the reaction progress during irradiation of **1** was analyzed by the method of "Evolving Factor Analysis (EFA)".[25] The method does not rely on a kinetic reaction model. Concentration changes are obtained from the weight of the linearly independent spectral components, which are determined iteratively for increasing irradiation doses. The result is shown in Figure 1. The spectrum of the first photoproduct, as estimated by EFA, is close to that of an authentic sample of 2-nitrosobenzaldehyde (**4**). The photoproduct was further identified by GC−MS analysis of the irradiated mixture and comparison with an authentic sample of **4**. On the other hand, irradiation of **2** induced essentially clean and complete conversion to **5**.
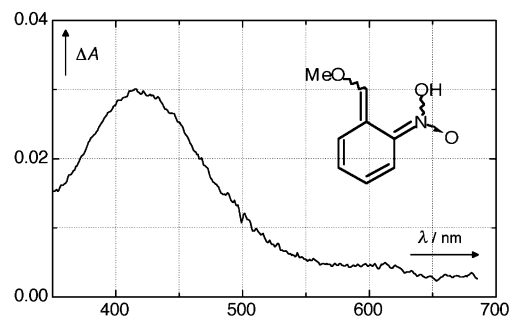
(20) Stephens, P. J.; Devlin, F. J.; Chabalowski, C. F.; Frisch M. J. *J. Phys. Chem.* **1994**, *98*, 11 623−11 627.
(21) Scott, A. P., Radom, L. *J. Phys. Chem.* **1996**, *100*, 16 502−16 513.
(22) Il'ichev, Y. V.; Wirz, J. *J. Phys. Chem. A* **2000**, *104*, 7856−7870.
(23) (a) Miertus, S.; Scrocco, E.; Tomasi, J. *Chem. Phys.* **1981**, *55*, 117−129. (b) Miertus, S.; Tomasi, J. *Chem. Phys.* **1982**, *65*, 239−245. (c) Cossi, M.; Barone, V.; Cammi, R.; Tomasi, J. *Chem. Phys. Lett.* **1996**, *255*, 327−335.
(24) Casida, M. E.; Jamorski, C.; Casida, K. C.; Salahub, D. R. *J. Chem. Phys.* **1998**, *108*, 4439−4449.
(25) Gampp, H.; Maeder, M.; Meyer, C. J.; Zuberbühler, A. D. *Talanta* **1986**, *33*, 943−951.

Figure 2. Transient absorption spectrum observed by picosecond pump−probe spectroscopy of **1** in acetonitrile.

Scheme 2: Intermediates Observed in the Photoreaction of 2-Nitrobenzyl Methyl Ether (**1**)
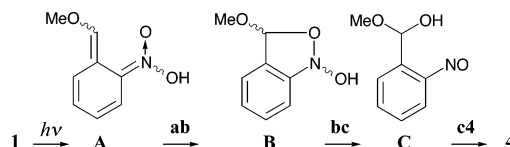
Quantum yields for the conversion of **1** to **4** ($\phi = 0.49 \pm 0.05$, aqueous acetate buffer 1:1, 3 measurements) and of **2** to **5** ($\phi = 0.48 \pm 0.05$, aqueous phosphate buffer $H_2PO_4^-$:HPO_4^{2-} = 1:1, 3 measurements) were determined spectrophotometrically ($\lambda_{exc} = 365$ nm, $\lambda_{obs} = 310$ nm) using azobenzene actinometry and assuming clean reactions of **1** to **4** and of **2** to **5** at low conversions. The extinction coefficients of **4** in water were determined with an authentic sample (Experimental Section). Those of 2-nitrosoacetophenone (**5**), λ_{max}/nm (log [ϵ/M^{-1} cm^{-1}]) 287 (3.78), 311 (3.82), 750 (1.3), were estimated from the essentially clean conversion of **2** to **5**. In the dark, the nitroso compounds **4** and **5** were stable for hours in the pH-range of 3−6, but decomposed at higher or lower acidities. The rate coefficients for the acid- and base-catalyzed decays of **4** were found to be $k_H \approx 20$ M^{-1} s^{-1} and $k_{OH} \approx 5 \times 10^5$ M^{-1} s^{-1}. The decomposition products were not investigated. The equilibrium with nitroso dimers lies far on the side of the monomers at the low concentrations ($<1 \times 10^{-4}$ M) used in these experiments.[26]

Picosecond Pump−Probe Spectroscopy. Broad transient absorption ($\lambda_{max} = 413$ nm, Figure 2) appeared within 5 ps after excitation of **1** with 248-nm subpicosecond pulses in acetonitrile and persisted up to the maximum delay of 1.8 ns. Similar results ($\lambda_{max} = 415$ nm) were obtained with **2**. The transient absorption is attributed to the *aci*-nitro tautomers formed by intramolecular hydrogen transfer in the singlet excited state. Only very weak absorption was observed at wavelengths > 550 nm, and no resolved growth of the *aci*-absorption due to a slower reaction via the triplet state of **1** or **2** could be detected. Such observations had been reported for related nitrobenzyl compounds.[27]

Nanosecond Laser Flash Photolysis (LFP) of 1. Five kinetically distinguishable transient intermediates were detected by nanosecond LFP of **1** in aqueous solution and in other solvents. For the following discussion the transient intermediates are labeled as **A**, **B**, and **C** (Scheme 2). Stereoisomers of **A** and **B** exhibiting different reaction kinetics are distinguished as **A1**

(26) Azoulay, M.; Wettermark, G. *Tetrahedron* **1978**, *34*, 2591−2596.
(27) Yip, R. W.; Sharma, D. K.; Giasson, R.; Gravel, D. *J. Phys. Chem.* **1984**, *88*, 5770−5772. Yip, R. W.; Sharma, D. K.; Giasson, R.; Gravel, D. *J. Phys. Chem.* **1985**, *89*, 5328−5330. Yip, R. W.; Sharma, D. K.; Giasson, R.; Gravel, D.; Wen, Y. X. *J. Phys. Chem.* **1991**, *95*, 6078−6081. Yip, R. W.; Sharma, D. K.; Giasson, R.; Gravel, D.; Blanchet, D. *Can. J. Chem.* **1991**, *69*, 1193−1200.
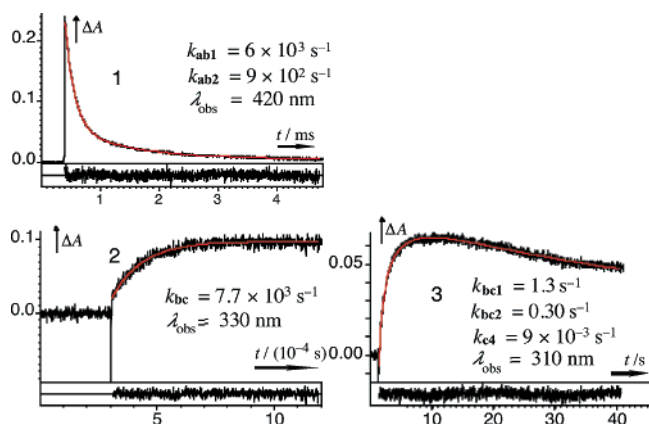
Figure 3. Kinetic traces obtained by LFP of **1** at 30 °C (for comparison with the FTIR measurements). Trace 1: Acetonitrile. Trace 2: Acetonitrile with 75 mM D$_2$SO$_4$. Trace 3: CH$_2$Cl$_2$.

Figure 4. pH−Rate profiles of reactions **ab1** (●), **ab2** (○), **bc1** (+), **bc2** (×), and **c4** (□) initiated by LFP of **1**. The solid lines were obtained by nonlinear least-squares fitting of eq 1 to the data points (Table S1)[30] for **ab1** and **ab2** and of eq 3 to those for **bc1**, **bc2**, and **c4**. The resulting parameters are given in Table 1.

and **A2** and as **B1** and **B2**. The identification of these transients as the *aci*-tautomers, **A**, or their anions, **A**⁻, 1,3-dihydrobenz-[*c*]isoxazol-1-ol intermediates, **B**, and hemiacetal, **C**, rests on the TRIR data, absorption spectra, pH-rate profiles, and observations of general acid and base catalysis reported below. Reaction **A1** → **B1** is labeled as **ab1**, **A2** → **B2** as **ab2**, and so on. The same symbols **A**−**C** will be used to designate the corresponding intermediates formed from **2** and **3**.

Nonaqueous Solvents. Excitation of **1** in acetonitrile by a nanosecond laser pulse (308 nm) produced transient **A** within the duration of the laser pulse. The spectrum of **A** was identical to that seen in the pump−probe experiment (Figure 2), and its decay obeyed a biexponential rate law, with rate constants k_{ab1} ≈ 6 × 10³ and k_{ab2} ≈ 9 × 10² s⁻¹ (trace 1 in Figure 3).[28] Reactions **ab1** and **ab2** were strongly accelerated in the presence of a mineral acid. They merged to a monoexponential decay, k_{ab} ≈ 3 × 10⁷ s⁻¹,[29] in the presence of 0.02 M H$_2$SO$_4$. The decays were also, but less strongly, accelerated by acetic acid (1.7 M), k_{ab1} ≈ 2 × 10⁵ and k_{ab2} ≈ 5 × 10⁴ s⁻¹.[28] For comparison with the TRIR experiments discussed below, the growth of absorbance at 310−330 nm (formation of **C**, vide infra) was measured by LFP of **1** in CH$_3$CN that was acidified with 75 mM D$_2$SO$_4$, k_{bc} = 7.7 × 10³ s⁻¹ (trace 2). LFP of **1** in CH$_2$Cl$_2$ showed biexponential growth of absorption at 310 nm (formation of **C**), k_{bc1} ≈ 1.3 and k_{bc2} ≈ 0.3 s⁻¹, and was followed by a slow decay of **C** to **4**, k_{c4} = 9 × 10⁻³ s⁻¹ (trace 3).

pH-Rate Profiles in Aqueous Solution. The absorption spectra of the *aci*-intermediates **A** observed immediately after LFP of **1** in aqueous solutions were similar to the pump−probe spectra obtained with **1** in acetonitrile (Figure 2), but the absorption maximum was shifted to slightly longer wavelength, λ_{max} = 420 nm. The decay of this transient absorption obeyed a biexponential rate law at pH > 5. The amplitudes of the two components were approximately equal.[28] The decay of the short-lived component was accompanied by a 15-nm blue shift of the absorption maximum (measured in phosphate buffer, pH 6.8). This indicates that transient **A** is a mixture of two kinetically distinct species, **A1** and **A2**.

(28) The decay traces clearly deviated from a simple first-order rate law and gave excellent fits with two exponentials, but the two close-lying rate constants and their amplitudes were not defined with high accuracy.
(29) This value is close to the time resolution of our instrument that was limited by the 30-ns duration of the laser pulse.
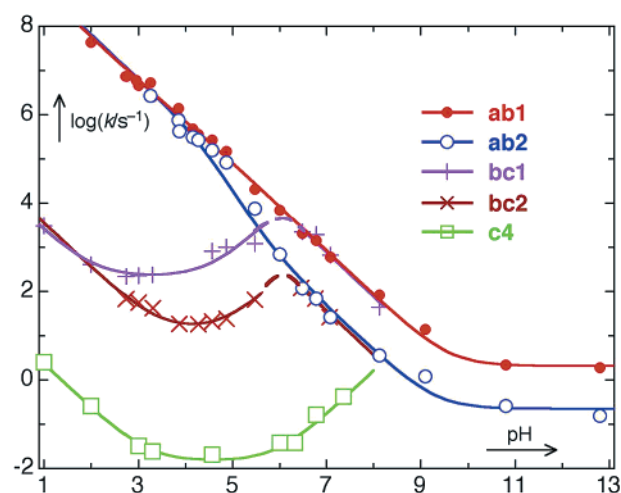
Rate constants determined with buffer solutions (pH 3.5−10.5) were found to increase linearly with buffer concentration indicating general acid and/or base catalysis. Data points for the pH-rate profile were, therefore, obtained by linear extrapolation of buffer dilution plots (vide infra) to zero buffer concentration. The pH-rate profiles for reactions **ab1** and **ab2** are shown in Figure 4. The data points are given in Table S1 of the Supporting Information.[30]

The rates of reactions **ab1** and **ab2** are constant at pH > 10, and rise steadily with increasing acid concentration at pH < 10. The slope of log k_{obs} for reaction **ab2** clearly drops below −1 in the pH range of 4−6. The solid lines were obtained by nonlinear least-squares fitting of the parameters k_{ab}'', k_{ab}', and $k_{ab}/K_{a,1}$ in eq 1 to the observed first-order rate constants of reactions **ab1** and **ab2**. Equation 1 will be derived in the Discussion. The acidity constants $K_{a,2}$ of **A1** and **A2** were more accurately defined by the buffer dilution plots (vide infra) and were thus fixed to the values $K_{a,2}(A1)$ = 3.2 × 10⁻⁵ M and $K_{a,2}(A2)$ = 1.0 × 10⁻⁴ M for fitting of eq 1.

$$\log (k_{obs}/s^{-1}) = \log\{(k_{ab}''K_{a,2} + k_{ab}'[H^+] + k_{ab}[H^+]^2/K_{a,1})/(M\ s^{-1})\} - \log\{([H^+] + K_{a,2})/M\}\ (1)$$

In pure water with no buffer added, a small time-resolved increase in absorbance was observed following the sudden rise in absorption at 420 nm. This is attributed to ionization of the *aci*-nitro transients **A** to the conjugate anions **A**⁻, k_{-H} = (2.7 ± 0.3) × 10⁶ s⁻¹ (ca 10% of the total amplitude), which appear to show stronger absorption at 420 nm. This rate constant is nearly an order of magnitude lower than that of the *aci*-tautomer of 2-nitrotoluene,[8] indicating that the acidity constants of the *aci*-tautomers **A**, $K_{a,2} = k_{-H}/k_H$, are about an order magnitude smaller than that of the latter, p$K_{a,2}$ = 3.6. Combination of k_{-H} with a typical rate constant for the reaction of protons with a weak oxygen base, k_H ≈ 5 × 10¹⁰ M⁻¹ s⁻¹, provides a first estimate of the acidity constant of the *aci*-tautomers **A**, p$K_{a,2}$ ≈

(30) Supporting Information: See paragraph at the end of this paper regarding availability.

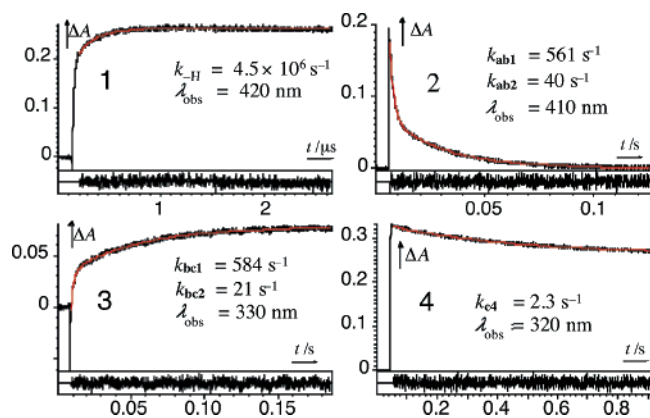**Figure 5.** Kinetic traces obtained by LFP of **1** in aqueous solutions. Trace 1: ionization of **A** in 5×10^{-4} M NaOH. Trace 2: decay of **A1** and **A2** in phosphate buffer (0.0143 M KH$_2$PO$_4$, 0.0286 M Na$_2$HPO$_4$, pH 7.08). Trace 3: reaction **bc1** and **bc2** in acetate buffer (0.0072M HAc, 0.00144 M NaAc, pH 3.87). Trace 4: reaction **c4** in 0.1 M HClO$_4$.

4.3.[31] Ionization of the *aci*-tautomers **A** was accelerated by the addition of NaOH or buffers. Measurements in the range of 5×10^{-4} (Figure 5, trace 1) to 1×10^{-3} M NaOH gave a rate constant of $k_{OH} = (8 \pm 2) \times 10^9$ M^{-1} s^{-1} for the deprotonation of **A** to **A**$^-$ by hydroxyl ions. A very weak transient absorption that was observed at 500 nm decayed with a rate constant of ca. 5×10^6 s^{-1}, independent of pH (up to 1 M NaOH) and oxygen (up to 1 atm). We cannot offer a convincing assignment for this transient.

The decay of transient **A** was clearly biexponential at pH > 5 (trace 2 in Figure 5). With increasing acidity the decay rate of the slower component **A2** increased more rapidly than that of **A1**, such that the two decays merged to an essentially single exponential with a rate constant of about 6×10^5 s^{-1} at pH 3 (cf., however, the buffer dilution plots discussed below). The absorption due to transients **A1** and **A2** decayed to the baseline in aqueous solutions with pH < 6, leaving no residual absorption above 300 nm. Subsequently, a slow, biexponential growth in absorbance was observed at 310–330 nm (trace 3 in Figure 5: formation of intermediate **C**). These observations require intervention of some intermediates, **B1** and **B2**, which are transparent above 300 nm. The pH-dependence of the two first-order rate constants for the formation of **C** from **B1** and **B2**, determined at 330 nm, is shown in Figure 4 (reactions **bc1** and **bc2**). Formation of **C** is also accompanied by the growth of a very weak absorbance at 740 nm, which is characteristic for the formation of nitroso compounds.[32] However, the measurements at 330 nm gave more accurate results, because the absorbance changes associated with the reactions **B** → **C** are much larger at this wavelength. The decay of transients **B** is catalyzed by base. At pH > 6 the decay rates of **B1** and **B2** exceed the rates of formation of these intermediates, so that the decay rates of **A1** and **A2** coincide with the rates of formation of **C**.

In general, the time-dependent concentration of a product **C** that is formed in a sequential reaction scheme of the type **A** → **B** → **C** with rate constants k_{ab} and k_{bc} is given by eq 2. Thus, the formation of **C** by the two parallel reaction sequences **A1**

(31) A similar estimate based on the ionization kinetics of 2-nitrotoluene's *aci*-nitro tautomer in pure water gave p$K_a \approx 3.4$, in good agreement with pK_a = 3.6 determined independently.[8]
(32) Walker, J. W.; Reid, G. P.; McCray, J. A.; Trentham, D. R. *J. Am. Chem. Soc.* **1988**, *110*, 7170–7177.
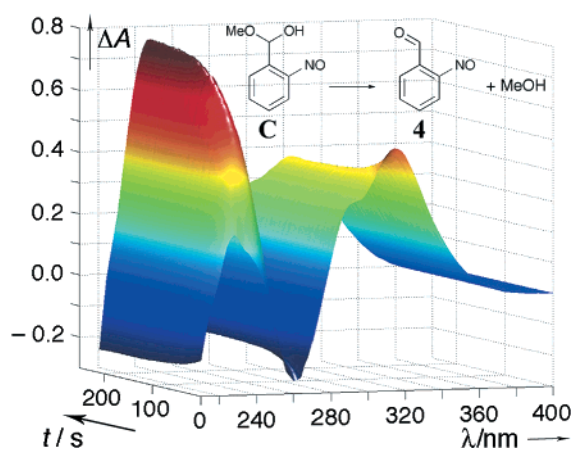
Figure 6. UV−vis difference absorbance spectra monitoring reaction **c4** in aqueous solution. The first spectrum was recorded about 10 s after LFP of **1** in 5×10^{-4} M HClO$_4$.

→ **B1** → **C** and **A2** → **B2** → **C** is expected to obey a four-exponential rate law.

$$[C]_t = [A]_{t=0} \frac{k_{bc}(1 - e^{-k_{ab}t}) - k_{ab}(1 - e^{-k_{bc}t})}{k_{bc} - k_{ab}} \quad (2)$$

However, eq 2 rapidly approaches a single-exponential rate law, $[C]_t \approx [A]_{t=0}(1 - e^{-kt})$, as the two rate constants k_{ab} and k_{bc} become different in magnitude, with the observable rate constant k becoming that of the slower (rate limiting) step. A reliable determination of four rate constants was not possible from the absorbance growth waveforms monitored at 330 nm. Growth curves determined in the pH range of 5.5−6.5, where $k_{ab} \approx k_{bc}$ and a four-exponential fit would have been required, were disregarded in the analysis. Traces obtained outside that range were adequately fitted by a sum of two exponentials (Figure 5, trace 3). The two rate constants for the formation of **C** that were determined at 330 nm in solutions of pH > 6.5 are limited by and equal to the rate constants of the reactions **ab1** and **ab2**, k_{ab1} and k_{ab2}, whereas those at pH < 5.5 are slower and provide the rate constants of reactions **bc**, k_{bc1}, and k_{bc2}.

Finally, the lifetime of product **C** is around 40 s in the pH-range of 3−6, and the absorbance changes arising from reaction **c4** were sufficiently slow to be recorded with a diode array UV spectrometer. The absorbance at 320 nm due to **C** decreases, while that at 230 nm increases strongly (Figure 6). A global fit of the data obtained with 5×10^{-4} M aqueous HClO$_4$ gave a rate constant of $(2.57 \pm 0.01) \times 10^{-2}$ s^{-1} and provided UV spectra of the initial ($t = 0$) and final species. These were nearly superimposable with the UV spectra of 2-nitrosobenzyl alcohol (as a stable analogue for the hemiacetal **C**) and authentic **4**, respectively, in the same solvent. The higher rate constants k_{c4} outside the range of 3 < pH < 6 were determined by kinetic flash photolysis analyzed at 320 nm.

The pH-rate profiles for reactions **bc1**, **bc2**, and **c4** (Figure 4) indicate acid catalysis at pH < 3 and base catalysis at pH > 5. Equation 3 describes a reaction that has a pH-independent

$$\log(k_{obs}/s^{-1}) = \log\{(k_H[H^+] + k_{OH}K_W/[H^+] + k_0)/s^{-1}\} \quad (3)$$

component, k_0, but also exhibits catalysis by protons, k_H, and by hydroxide ions, k_{OH}. The hydroxyl ion concentration was replaced by $K_W/[H^+]$, where $K_W = 1.59 \times 10^{-14}$ M^2 is the

Table 1. Rate Coefficients Determined by Fitting of Eqs 1 and 3 to the pH-Rate Profiles of **1** to **3**

reaction	k_{ab}''/s^{-1}	k_{ab}'/s^{-1}	$(k_{ab}/K_{a,1})/\text{s}^{-1}$	$K_{a,2}/\text{M}$
ab1(1)	2.1 ± 0.4	$(8.7 \pm 0.8) \times 10^5$	$(5.0 \pm 0.6) \times 10^9$	$\sim 1.0 \times 10^{-4a,b}$
ab2(1)	0.23 ± 0.08	$(1.4 \pm 0.3) \times 10^4$	$(7.8 \pm 1.5) \times 10^9$	$\sim 3.2 \times 10^{-5a,b}$
ab1(2)		$(5.1 \pm 0.2) \times 10^7$	$\sim 7 \times 10^9$	
ab2(2)	$(9 \pm 2) \times 10^2$	$(1.1 \pm 0.2) \times 10^6$	$(1.8 \pm 0.8) \times 10^{10}$	1×10^{-4b}
ab(3)	1.5 ± 0.5	$(7 \pm 2) \times 10^4$	$\sim 5 \times 10^9$	3.2×10^{-5b}

reaction	$k_{H}/\text{M}^{-1}\,\text{s}^{-1}$	k_0/s^{-1}	$k_{OH}/\text{M}^{-1}\,\text{s}^{-1}$
bc1(1)	$(2.6 \pm 0.4) \times 10^4$	$(1.8 \pm 0.2) \times 10^2$	$\sim 1 \times 10^{10}$
bc2(1)	$(3.6 \pm 0.3) \times 10^4$	13 ± 2	$(1.1 \pm 0.2) \times 10^{10}$
c4(1)	23 ± 4	$(1.6 \pm 0.3) \times 10^{-3}$	$(1.2 \pm 0.2) \times 10^6$
bc(2)	$\sim 1 \times 10^3$	$(4.0 \pm 2.7) \times 10^2$	$\sim 1 \times 10^{10}$
c5(2)	$(2.3 \pm 0.9) \times 10^2$	$\sim 1 \times 10^{-2}$	$\sim 1.3 \times 10^6$
bc(3)	$(2.0 \pm 0.2) \times 10^7$	$(7.7 \pm 0.9) \times 10^3$	

a Value taken from a fit of buffer slopes to eq 5. *b* Value was kept constant in fitting.
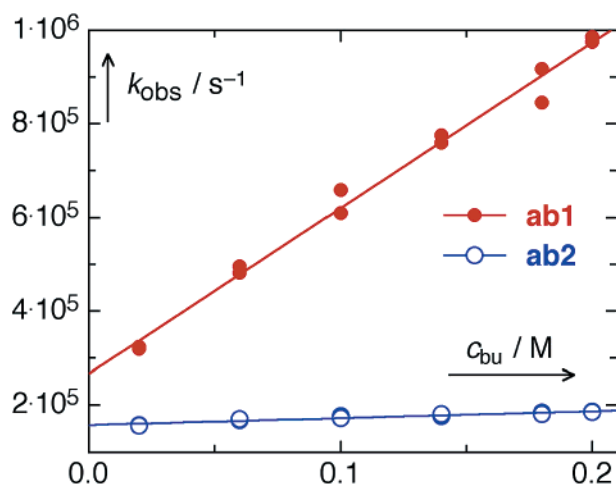
Figure 7. Buffer dilution plot for the decay rate constants of transients **A1** (●) and **A2** (○) in acetic acid buffer 1:1 (pH 4.57).

ionization constant of water at ionic strength $I = 0.1$ M.[33] Nonlinear least-squares fitting of eq 3 to the observed rate constants for reactions **bc1**, **bc2**, and **c4** provided the parameters k_0, k_H, and k_{OH} for each reaction, which are given in Table 1. The coincidence of the reaction rates for **ab1** and **bc1** and for **ab2** and **bc2** at pH > 6 (Figure 4) proves that intermediate **A1** is the precursor of **B1**, and **A2** of **B2**. Consistently, the amplitude ratio of reactions **ab1** and **ab2** in the kinetic traces measured at 420 nm was about equal to that of reactions **bc1** and **bc2** at 320 nm.

Buffer Dilution Plots. Measurements in aqueous solutions of pH 3.5−10.5 require the addition of buffers, which, however, may influence the reaction rates by general acid and general base catalysis. These measurements were made in series of solutions of varying buffer concentration but constant buffer ratio and, hence, constant pH. Catalysis by buffers was found for all reactions and buffer dilution plots at constant buffer ratio were linear (e.g., Figure 7). The intercepts represent the decay rates at zero buffer concentration, which were used for the pH-rate profiles (Figure 4). The buffer catalytic coefficients, k_{bu}, which correspond to the slopes of the buffer dilution plots, are given in Table 2. As shown in Figure 7, the slopes k_{bu} determined for the decay of **A1** were about 10-fold higher than

(33) Bates, R. G. *Determination of pH, Theory and Practice*; Wiley: New York, 1973.

those of **A2**. This led to a clear-cut separation of the two reaction rates with increasing buffer concentration in acetic and formic acid buffers, and proves that the near coincidence of the decay rate constants k_{ab1} and k_{ab2} in wholly aqueous solutions at pH < 5 is fortuitous.

Solvent Kinetic Isotope Effects. The decay rates of **A1** and **A2** were determined in H_2O and D_2O solutions with equal nominal concentration of added acid or base: $k^H/k^D = 0.97 \pm 0.03$ in 1.1×10^{-3} M aqueous perchloric acid (single exponential), and $k^H/k^D = 1.08 \pm 0.18$ (**ab1**) and 0.84 ± 0.18 (**ab2**) in 0.1 M sodium hydroxide. Relatively large error limits in the latter values arise because of the uncertainty associated with fitting decay traces with a sum of two close-lying exponentials.

TRIR-Measurements of 1. The IR-spectrum of **1** in CD_3-CN is dominated by strong bands arising from the symmetric (1343 cm^{-1}) and antisymmetric (1526 cm^{-1}) stretching vibrations of the NO_2 group. Medium intensity bands are seen in the range 2800−3000 cm^{-1} (C−H stretch) and at 1109 cm^{-1} (antisymmetric C−O−C stretch). The corresponding frequencies predicted by the DFT calculations (1329 and 1353 cm^{-1} for the symmetric NO_2 stretch, 1551 and 1564 cm^{-1} for the antisymmetric NO_2 stretch, 1109 and 1111 cm^{-1} for the C−OMe stretch in the *anti-* and *syn*-conformations of **1**, respectively) are in satisfactory agreement with the experimental data.

CD_3CN and CD_2Cl_2 were used as solvents for the TRIR experiments. Measurements with the same (nondeuterated) solvents were done by optical LFP for comparison. Reaction **A** → **B** in CD_3CN was followed by the step-scan method with a 9×10^{-3} M solution of **1**. The kinetic analysis of TRIR spectral data is less precise than that of kinetic traces obtained by optical LFP and the TRIR data for reactions **ab** and **bc** were adequately fitted with a single exponential function. Hence, only a single IR spectrum is available for **A** (representing a mixture of **A1** and **A2**), and one for **B**.

Reaction A → B. The spectral matrix covering a time range from 2.5 to 500 μs after flash photolysis (Figure 8) was subjected to factor analysis. Two components were sufficient to reconstruct the spectra within experimental accuracy. Prominent features are the decaying bands in the region of 1100−1400 and 1540−1650 cm^{-1}. A band at 1080 cm^{-1} grows in simultaneously, but otherwise no strong absorption bands, particularly no N=O or C=O bands, are present in the last spectra. The strong negative bands in the difference spectra did not show a significant change in position or intensity during the time span covered. The positions of these negative bands correspond to those of the absorption bands of **1** indicating depletion of the starting material **1**.

Intermediates A. The data matrix represented in Figure 8 was adequately fitted by a single-exponential rate law. The resulting rate constant $k_{ab} = (6.6 \pm 0.2) \times 10^3$ s^{-1} is in good agreement with that for the major component, $k_{ab1} \approx 6 \times 10^3$ s^{-1},[28] of the biexponential decay observed by LFP of **1** in acetonitrile. The negative bands due to the depletion of **1** were removed by adding an appropriate amount of the IR spectrum of **1** to the first spectrum of Figure 8 to obtain the absorption spectrum of transients **A**, Figure 9. It is in qualitative agreement with the much more highly resolved spectrum that was reported by Dunkin et al.[34] for the same product formed by irradiation of **1** in Ar and N_2 matrixes at 12 K.

Table 2. Buffer Slopes k_{Bu} Obtained with **1** by Linear Regression of Buffer Dilution Plots[a]

buffer	x_{HB}	c_{bu}/M[b]	$k_{bu}^{ab1}/(M^{-1}s^{-1})$	$k_{bu}^{ab2}/(M^{-}s^{-1})$	$k_{bu}^{bc1}/(M^{-1}s^{-1})$	$k_{bu}^{bc2}/(M^{-1}s^{-1})$	$k_{bu}^{c4}/(M^{-1}s^{-1})$
phthalic	1/2	0.01−0.05	$(2.70 \pm 0.45) \times 10^{7c}$	c	$(7.1 \pm 0.7) \times 10^3$	$(4.5 \pm 0.6) \times 10^2$	
formic	4/5	0.05−0.50	$(4.8 \pm 0.3) \times 10^{6c}$	c			
formic	2/3	0.03−0.30	$(6.2 \pm 1.9) \times 10^7$	$(5.0 \pm 0.3) \times 10^6$			
formic	1/3	0.015−0.15	$(3.1 \pm 0.3) \times 10^6$	$(1.9 \pm 0.2) \times 10^6$			
formic	1/5	0.0125−0.125	$(1.3 \pm 0.1) \times 10^7$	$(1.4 \pm 0.1) \times 10^6$			
acetic	5/6	0.011−0.60	$(1.18 \pm 0.03) \times 10^7$	$(1.16 \pm 0.14) \times 10^6$	$(2.9 \pm 0.2) \times 10^4$	143 ± 9	
acetic	2/3	0.02−0.12	$(7.6 \pm 1.1) \times 10^6$	$(4.5 \pm 1.2) \times 10^5$	$(7.2 \pm 0.3) \times 10^4$	261 ± 18	
acetic	1/2	0.02−0.2	$(3.5 \pm 0.1) \times 10^6$	$(1.46 \pm 0.13) \times 10^5$	$(1.10 \pm 0.05) \times 10^5$	287 ± 17	0.09 ± 0.03
acetic	1/3	0.015−0.15	$(1.1 \pm 0.1) \times 10^6$	$<6 \times 10^3$	$(1.5 \pm 0.1) \times 10^5$	385 ± 19	
acetic	1/9	0.01−0.11	$(5.8 \pm 1.0) \times 10^4$	$<6 \times 10^4$	$(1.1 \pm 0.1) \times 10^5$	431 ± 46	
phosphate	6/7	0.008−0.078	$(8.6 \pm 3.8) \times 10^3$	$(1.9 \pm 0.1) \times 10^4$	d	$(5.9 \pm 0.5) \times 10^3$	
phosphate	3/4						1.5 ± 0.4
phosphate	2/3	0.015−0.060	$(1.5 \pm 1.0) \times 10^3$	$(3.6 \pm 0.2) \times 10^3$	$<3 \times 10^3$	$(3.4 \pm 0.2) \times 10^3$	
phosphate	1/2	0.005−0.050	$<7 \times 10^3$	$(1.4 \pm 0.2) \times 10^3$	$<5 \times 10^3$	$(1.4 \pm 0.2) \times 10^3$	<1
phosphate	1/3	0.011−0.043	$<1 \times 10^3$	$(3.2 \pm 0.1) \times 10^2$	$<2 \times 10^3$	$(4.5 \pm 0.8) \times 10^2$	
tris	1/2	0.02−0.2	<50	6 ± 3	55 ± 14		
borate	1/2	0.01−0.05	<50	<5			

[a] Experimental data are given in Table S4[30]. [b] Total buffer concentration, $[HB] + [B^-]$. [c] The decay rates of **A1** and **A2** were too close to be separated. [d] The buffer dilution plot was nonlinear, because reaction **ab1** becomes rate-limiting at high buffer concentrations (Figure 4).
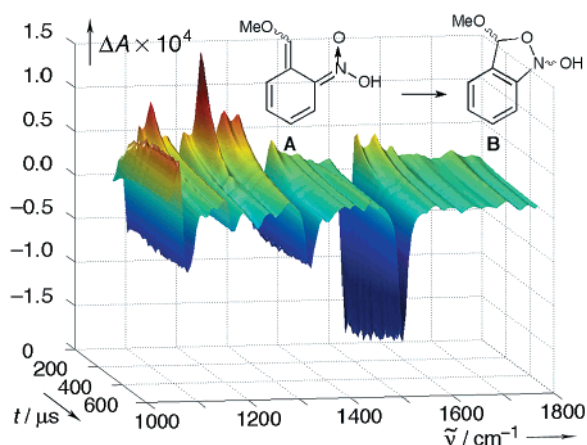

Figure 8. TRIR difference spectra of **1** in CD₃CN measured by the step-scan technique. Time after excitation increases from back to front.
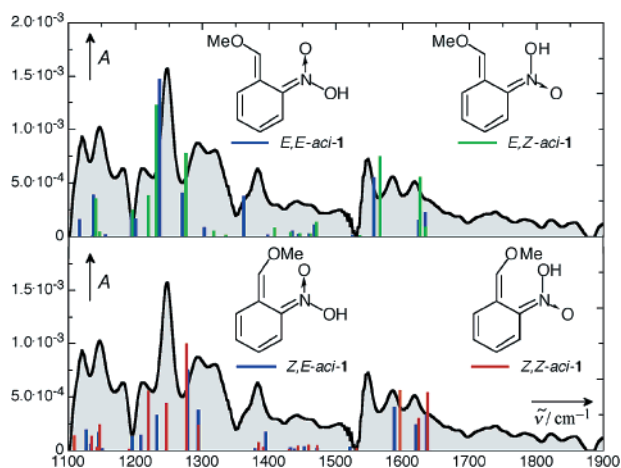

Figure 9. IR spectrum of intermediates **A** (both upper and lower) determined by adding an appropriate amount of the IR spectrum of **1** to the initial TRIR difference spectra of Figure 8. Vertical bars indicate IR frequencies and intensities predicted by DFT calculations for the four isomers of *aci*-**1** (Table S5).[30] The first label (*E* or *Z*) denotes the configuration of the exocyclic C=C bond, the second that of the C=N bond.

Dunkin et al.[34] attributed their matrix spectrum to the *E,E*-isomer of *aci*-**1**. Spectra for all four possible isomers of *aci*-**1** were calculated with DFT techniques (Table S5).[30] An identification of structural isomers based on the solution spectrum,

Figure 9, is hardly warranted, but the *E,E*-isomer appears to be present in significant amount, because strong absorption in the range 1350−1400 cm⁻¹ was predicted only for this isomer. The three bands in the 1550−1650 cm⁻¹ region suggest that other isomers are also formed. The biexponential decay kinetics observed for transient **A** (Figures 3 and 5, cf. Discussion) indeed indicates formation of at least two geometrical isomers of **A** as primary photoproducts in solution, whereas the rigid environment in an argon matrix appears to favor formation of a single isomer. From the qualitative agreement of the IR-spectrum of **A** in acetonitrile with the matrix spectrum reported by Dunkin et al. and with the calculations, it is clear that the nitronic acids **A** do not ionize in acetonitrile. The IR spectra calculated for the two *aci*-anions **A⁻** (Table S6)[30] are substantially different.

Methyl vinylethers commonly show a strong asymmetric C−O−C stretching band around 1200 cm⁻¹. According to our DFT calculations the strongest feature in the IR spectra of the *E,E*- and *E,Z*-isomers of *aci*-**1** (1230−1245 cm⁻¹) corresponds to the C−OMe stretch. Thus the band observed at 1248 cm⁻¹ is attributed to this mode. The next strong band in the spectrum can be assigned to the NOH bending mode, which is predicted to be located in the 1270−1293 cm⁻¹ region. The band at 1211 cm⁻¹ was attributed to the NO stretching vibration which is strongly coupled to ring deformations according to the DFT results. The calculated frequencies for the N−OH stretch vary from 928 to 952 cm⁻¹ (outside the range covered). The strong band at 1144 cm⁻¹ seems to arise from the ring CH bending vibrations and CH₃ deformation modes. Our assignment of the C=C and C=N bands differs from that of Dunkin et al.[35] We attribute the 1620-cm⁻¹ band to the C=N group, the band at 1550 cm⁻¹ to the exocyclic C=C(O) group, and the 1580-cm⁻¹ band to skeletal double bond stretching.

Intermediates B. Transients **B** do not absorb in the near UV. In time-resolved optical measurements their presence was inferred only from the delayed formation of product **C**. The IR spectrum of **B** (Figure 10) was obtained by addition of the

(34) Dunkin, I. R.; Gebicki, J.; Kiszka, M.; Sanin-Leira, D. *J. Chem. Soc., Perkin Trans. 2* **2001**, 1414−1425. Dunkin, I. R.; Gebicki, J.; Kiszka, M.; Sanin-Leira, D. *Spectrochim. Acta, Part A* **1997**, *53A*, 2553−2557.
(35) Three bands are observed in the range of 1500−1650 cm⁻¹ (1550, 1580, 1620 cm⁻¹). The band at 1550 cm⁻¹ would be unusually low for either a C=C or a C=N stretching band. Additional conjugation tends to lower the position of C=N bands less than that of C=C bands (ref 37). Our DFT calculations predict the C=N stretching vibrations near 1620 cm⁻¹.
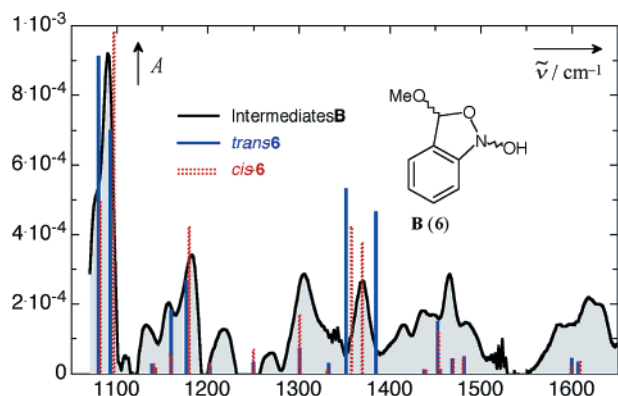
Figure 10. IR−Spectrum of intermediates **B** determined by adding an appropriate amount of the IR spectrum of **1** to the final TRIR difference spectra of Figure 8. Vertical bars indicate IR frequencies and intensities predicted by DFT calculations for the two isomers cis-**6** (red, dotted) and trans-**6** (blue).
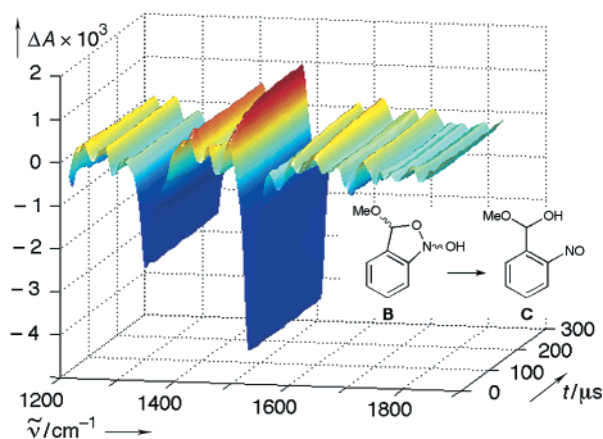

Figure 11. TRIR difference spectra of **1** in CD₃CN with 75 mM D₂SO₄. Time evolution is from front to back.

spectrum of depleted **A** to the last spectrum of Figure 8. It shows only one prominent band at 1080 cm^{-1}. Indeed, DFT-calculations for the two isomers of 3-methoxy-1,3-dihydrobenz[c]-isoxazol-1-ol (**6**) predict only one strong band (O−CH₃ stretch) located around 1100 cm^{-1}. The two other features in the predicted IR spectra around 1180 and 1370 cm^{-1} also coincide with observed bands. Dunkin et al.[34] report that irradiation of aci-**1** in an argon matrix yields a product with weak bands at 1637, 1091, and 756 cm^{-1}, which they attributed to the formation of **6**. The most important aspect in the spectrum of **B** is the *lack* of any strong bands in the range of 1400−1700 cm^{-1} that would indicate the presence of a C═O or an N═O group. Thus, our assignment of **B** to the cyclic intermediate **6** rests mainly on the subsequent evolution of the TRIR spectra described below.

TRIR spectroscopy of **1** in CD₃CN containing 75 mM D₂-SO₄ showed partially resolved growth of an N═O band at 1500 cm^{-1} (Figure 11), but still no absorption indicating the formation of a carbonyl group. Hence, reaction **B** → **C** is attributed to ring opening of the bicyclic compound **6** yielding the hemiacetal methoxy-(2-nitrosophenyl)-methanol (**7**). The rate constant, k_{bc} = (1.1 ± 0.1) × 10^4 s^{-1}, is in reasonable agreement with that obtained by LFP in the same medium, k_{bc} = 7.7 × 10^3 s^{-1} (Figure 3, trace 2).

Reaction C → 4. The final reaction **c4** was followed by fast-scan IR spectroscopy following 266-nm excitation of **1** in CD₂-
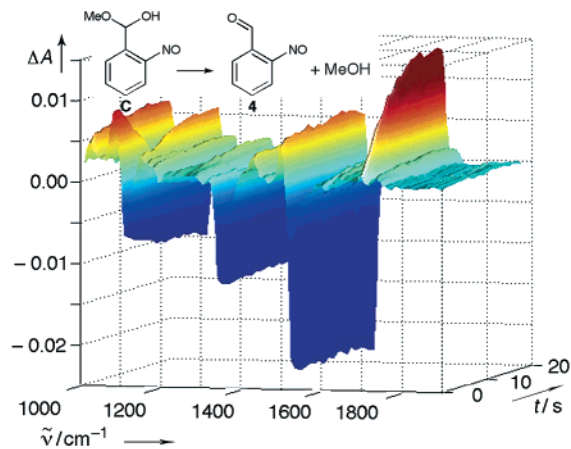

Figure 12. Fast-scan IR difference spectra of **1** in CD₂Cl₂.
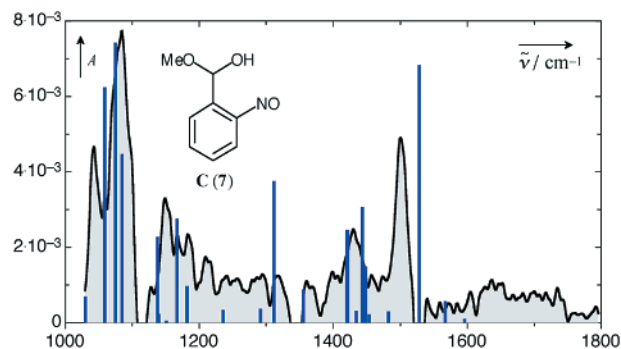

Figure 13. IR-spectrum of intermediate **C** in aqueous solution determined by adding an appropriate amount of the IR spectrum of **1** to the initial TRIR difference spectra of Figure 12. IR frequencies and intensities predicted by DFT calculations for the hemiacetal **7** are shown as vertical bars.

Cl₂. Figure 12 shows the resolved growth of an intense C═O band at 1700 cm^{-1}. The N═O band is fully developed already in the first spectrum, and its intensity hardly changes during the reaction, but its position gradually shifts from 1495 to 1501 cm^{-1} as the C═O band develops. Global analysis of the spectral matrix gave two significant components and their temporal evolution was fitted well by a first-order rate law. The resulting rate constant, k_{c4} = 1.3 × 10^{-2} s^{-1}, is close to that observed by LFP in the same solvent, k_{c4} = 9 × 10^{-3} s^{-1} (Figure 3, trace 3).

Removal of the negative peaks that are due to depletion of **1** from the first spectrum of Figure 12 provided the IR spectrum of **C** (Figure 13), which is shown together with the calculated frequencies for the conformer with an H-bond between the OH group and the oxygen atom of the NO group. This conformer is expected to be the primary product produced by ring-opening of cis-**6**.[22,36] A similar experimental spectrum of **C** (not shown) was obtained from the last spectrum of Figure 11.

The IR spectrum of the final photoproduct **4** (Figure 14) was obtained by correction for depleted **1** in the last spectrum of Figure 12. Comparison with the spectrum of authentic 2-nitrosobenzaldehyde (**4**) unambiguously identifies the end product as **4**. The band positions and intensities calculated for **4** (Table S6)[30] are in satisfactory agreement with experiment.

Further support for the assignment of intermediate **C** to the hemiacetal **7** stems from the IR spectral changes observed in

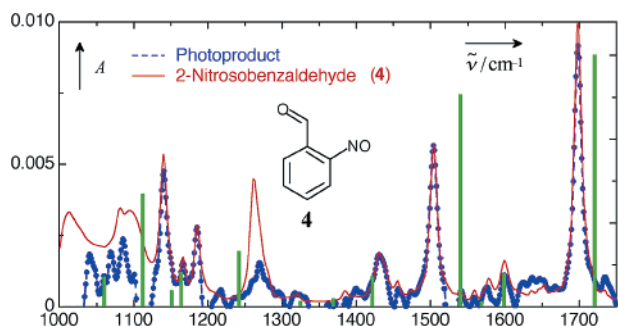(36) Il'ichev, Y. V. *J. Phys. Chem. A* **2003**, *107*, 10 159−10 170.

Figure 14. IR-spectrum of photoproduct of **1** (final spectrum of Figure 12, blue dotted line) compared to a spectrum of authentic 2-nitrosobenzaldehyde (**4**) in CD_2Cl_2 (solid red line). IR frequencies and intensities predicted by DFT calculations for **4** are shown as vertical bars.
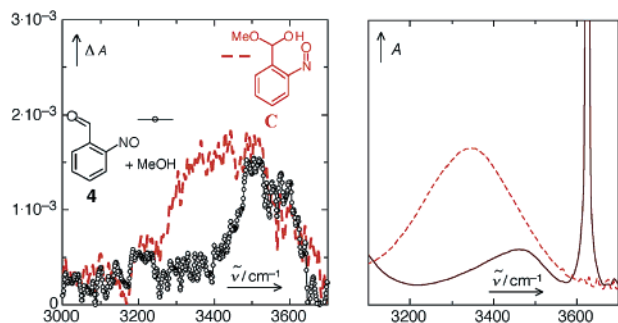

Figure 15. Left-hand graph: IR spectra of **C** (- − -, red) and of the final products **4** and methanol (-O-, black) in the range of 2500−3800 cm^{-1} obtained by TRIR. Right-hand graph: IR spectra of methanol (- − -, red) and dilute methanol in CD_2Cl_2 (solid black line).

the OH-stretch region during the conversion of **C** to **4** in CD_2-Cl_2. As shown in the left-hand part of Figure 15, the broad OH band of **C** ranging from 3200 to 3600 cm^{-1} changes to a substantially narrower band at 3500 cm^{-1} in the last spectrum. The broadness of the OH band of **C** is attributed to intramolecular H-bonding in the hemiacetal **7** and its narrowing in the course of the reaction **C** → **4** to the release of methanol. Only quite low concentrations of methanol are released in the IR experiment, so that it will not form H-bonded methanol clusters. The OH stretch bands of H-bonded alcohols are generally broad and lie at lower frequencies than those of the free species.[37] To illustrate the band shift and broadening resulting from the association of alcohols, the spectrum of a dilute solution of methanol in CD_2Cl_2 is compared to a spectrum of neat methanol in the right-hand part of Figure 15.

LFP of 2. The pH-rate profiles for the transients **A**, **B**, and **C** produced by LFP of **2** in aqueous solution are shown in Figure 16. The decays of the *aci*-transients **A** are biexponential with roughly equal amplitudes of the two components at 420 nm. Only one of the *aci*-decays, **A2**, is pH-dependent. The faster, pH-independent component **A1** absorbs at longer wavelengths; its amplitude dominates over that of **A2** at λ_{obs} > 420 nm. The decay rate of **A2** approaches a constant value around pH 4, but re-accelerates below pH 3, so that it escapes detection by nanosecond LFP at pH < 2.6. The decay rates for **A2** were fitted with eq 1 and the resulting parameters are given in Table 1. The growth of product **C** at 320 nm was monoexponential at pH < 6, exhibiting both acid and base catalysis. The parameters resulting from a fit with eq 3 are given in Table 1. At pH > 8,

(37) Bellamy, L. J. *The Infrared Spectra of Complex Molecules*, 3rd ed.; Chapman and Hall: London, 1975.
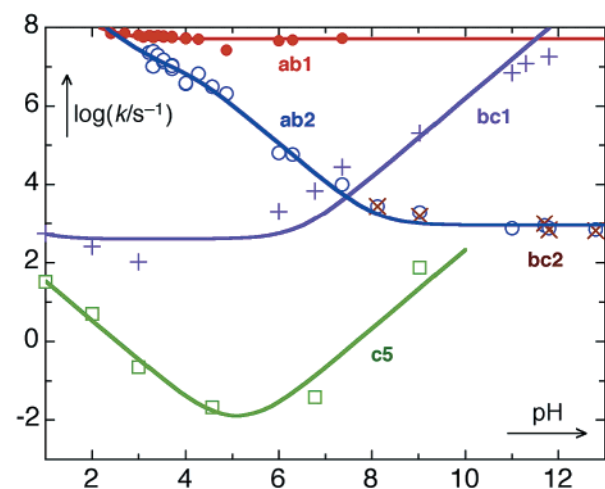

Figure 16. pH-Rate profiles of reactions **ab1** (●), **ab2** (○), **bc1** (+), **bc2** (×), and **c5** (□) initiated by LFP of **2**. The data points are given in Table S2.[30] The solid lines were obtained by nonlinear least-squares fitting of eq 1 for reactions **ab1** and **ab2** and of eq 3 for reactions **bc1**, **bc2**, and **c5**. The resulting fit parameters are given in Table 1.

formation of **C** occurs in two waves, the slower one being limited by the decay of the precursor **A2** in basic solutions. The rate of the faster component, **bc1**, increased linearly with increasing base concentration up to about pH 12, where its amplitude vanished and that of the slow component, **bc2**, was doubled. The slopes of buffer dilution plots are given in Table 3. The intrinsic decay rate constant of **A1**, $k_{ab1} = 5.1 \times 10^7$ s^{-1} is too fast to be affected by the acidic buffers. The decay of **A2** exhibits general acid catalysis, the formation of **C** general base catalysis (Table 3).

Caged ATP (3). LFP (351 nm, pulse energy 100 mJ) of **3** (10^{-4} M) was done in aqueous solutions at various pH. Buffer concentrations were kept sufficiently high to damp any effect of the disodium salt **3** on pH, but as low as possible to avoid buffer catalysis. The rate constants for the first-order decay of intermediate **A** (*aci*-**3**) were measured at 420 nm. The formation of the 2-nitrosophenyl chromophore (**C** or **5**) was monitored at 320 nm (Figure 17, Table S3).[30] It was delayed with respect to the *aci*-decay at pH < 6, indicating the intervention of a bicyclic intermediate **B** that does not absorb above 300 nm. The acidity constant of **A**, $K_{a,1}$, was not adequately defined by the rate data (Table S3),[30] and was therefore fixed at $pK_{a,1} = 4.5$. Nonlinear least-squares fitting of eqs (1) and (3) to the rate data for reactions **ab** and **bc**, respectively, gave the fitting parameters listed in Table 1.

Discussion

We begin with a brief review of previous mechanistic studies of the disodium salt of adenosine-5′-triphosphate-[P^3-(1-(2-nitrophenyl)ethyl)] ester (**3**, ′caged ATP′), which was introduced by Kaplan et al.[5] The first detailed study of the reaction mechanism of **3** was reported by Walker et al.[32] The decay rates of the *aci*-nitro intermediate were monitored by its absorption at 400 nm, and appearance rates were determined for each of the three products formed by LFP of **3**, namely ATP (bioassay), 2-nitrosoacetophenone (absorption at 740 nm), and H$^+$ (indicator dye). Two steps were kinetically resolved in aqueous solution at neutral pH. A fast step indicated release of a proton due to ionization of *aci*-**3** to **3**$^-$. In a slower reaction, $k = 86$ s^{-1} (pH 7.1, 21 °C), the free nucleotide and the side product 2-nitroso-

Table 3. Buffer Slopes k_{Bu} Obtained with **2** by Linear Regression of Buffer Dilution Plots[a]

buffer	x_{HB}	c_{bu}/M[b]	$k_{bu}^{ab2}/(M^{-1}s^{-1})$	$k_{bu}^{bc2}/(M^{-1}s^{-1})$	$k_{bu}^{c4}/(M^{-1}s^{-1})$
acetic	2/3	0.01−0.2	$(3.0 \pm 0.4) \times 10^8$	$(3.6 \pm 0.1) \times 10^4$	
acetic	1/2	0.02−0.2	$(2.2 \pm 0.3) \times 10^7$	$(5.2 \pm 0.4) \times 10^4$	0.09 ± 0.03
acetic	1/3	0.01−0.15	$(1.19 \pm 0.03) \times 10^8$	$(6.9 \pm 0.2) \times 10^4$	
phosphate	6/7	0.01−0.08	$(9.1 \pm 0.8) \times 10^6$	$(1.34 \pm 0.02) \times 10^6$	
phosphate	3/4	0.01−0.07	$(7.7 \pm 0.7) \times 10^6$	$(2.3 \pm 0.2) \times 10^6$	
phosphate	1/2	0.005−0.05	$(4.4 \pm 0.1) \times 10^6$	$(3.1 \pm 0.2) \times 10^6$	0.3 ± 0.2
phosphate	1/4	0.03−0.04	$(2.4 \pm 0.1) \times 10^6$	$(2.5 \pm 0.3) \times 10^6$	
tris	1/2	0.02−0.2	$(7.0 \pm 0.3) \times 10^4$	$(8.4 \pm 0.5) \times 10^4$	
borate	1/2	0.005−0.05	$(4 \pm 1) \times 10^4$	$(4.4 \pm 0.8) \times 10^4$	

[a] Experimental data are given in Table S4.[30] [b] Total buffer concentration, [HB] + [B⁻].
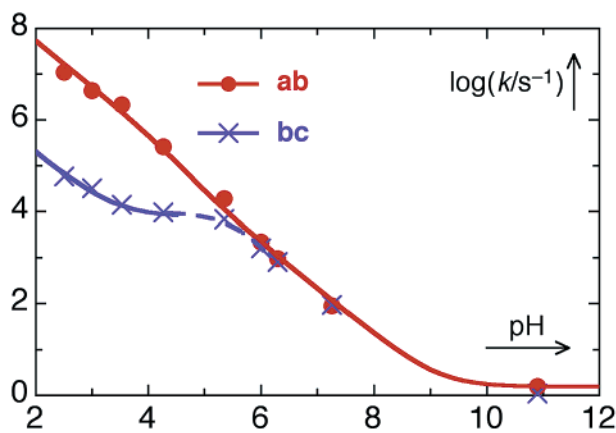
Figure 17. pH-Rate profiles for the dark reactions initiated by LFP of **3**.

Scheme 3: Reaction Mechanism Proposed[32] for Caged ATP (**3**)
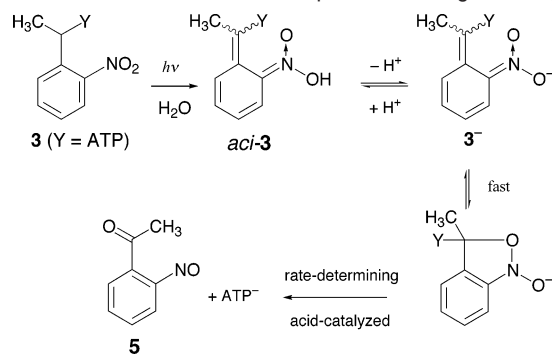
acetophenone (**5**) were formed concomitantly with the decay of **3⁻**. An important conclusion of this work was that the release rate of ATP coincides with the decay of the *aci*-anion **3⁻** under the conditions of the experiment. This finding was since corroborated by time-resolved IR[38] and by photoacoustic spectroscopy.[39] The reaction mechanism shown in Scheme 3 was proposed to explain the results.

Cyclization of **3⁻** was assumed to be fast but reversible, followed by rate-determining elimination of ATP. Acid catalysis on the observed decay rate of **3⁻** was attributed to protonation of the triphosphate substituent, thereby accelerating its elimination from the cyclic intermediate. Walker et al.[32] carefully declared their hypothesis as a minimal scheme to explain their results on caged ATP (**3**), and in a later review the same authors have expressed doubt about its generality.[40] Nevertheless, many

authors, including ourselves,[41] have implicitly or explicitly assumed this mechanism to hold in general, and the *aci*-decay rates were taken to indicate substrate release rates.

Several groups have questioned the validity of Scheme 3 in recent years. Ab initio and density functional theory calculations for the potential energy surface of 2-nitrotoluene and its isomers predicted a much higher activation barrier for cyclization of the *aci*-anion than for the neutral *aci*-tautomer.[22] These calculations also predicted cyclization of the neutral *aci*-tautomer to be highly exothermic, i.e., irreversible, whereas that of the anion was calculated to be endothermic. Similar conclusions were independently reached on the basis of semiempirical AM1 calculations for several 2-nitrobenzyl derivatives.[42] *This suggested that the observed acid catalysis arises from a rapid preequilibrium of* **3⁻** *with its conjugate acid* aci-**3**, *whereby the concentration of the reactive species* aci-**3** *increases with increasing acidity.* Experimental support for this hypothesis comes from a recent paper by Walbert et al.,[43] who studied 2-(2-nitrophenyl)-ethyl cages. From the dependence of the product distribution on pH they concluded that cyclization of their compounds proceeds only from the neutral *aci*-tautomer.

The present study deals with 2-nitrobenzyl (**1**) and 1-(2-nitrophenyl)ethyl methyl ether (**2**), which are transformed to 2-nitrosobenzaldehyde (**4**) and 2-nitrosoacetophenone (**5**), respectively, releasing methanol with quantum yields of about 50%. A brief reinvestigation of caged ATP (**3**) follows.

TRIR Measurements with 1. Three transient intermediates, **A**−**C** (Scheme 2), were detected by time-resolved infrared spectroscopy (TRIR) of **1** in aprotic solvents. The first transient, **A**, was formed within a μs after excitation of **1** in acetonitrile (Figure 8) and is attributed to *aci*-**1**. The characteristic absorption bands due the *aci*-nitro group (1100−1400 and 1540−1650 cm⁻¹, Figure 9) disappeared within 1 ms (reaction **ab**) leaving a single prominent IR band at 1080 cm⁻¹, which is attributed to the cyclic intermediate 1,3-dihydrobenz[c]isoxazol-1-ol (**B**). The observed spectrum of **B** agrees well with theoretical predictions, but its assignment rests mainly on the fact that the bands characteristic for the nitroso and carbonyl group appear only in the subsequent reactions. Ring opening of **B** yields the hemiacetal **C** (reaction **bc**, Figure 11). The IR spectrum of **C** (Figure 13) shows the presence of a nitroso group (1500 cm⁻¹), but carbonyl absorption is still lacking. Finally, formation of

(38) Barth, A.; Hauser, K.; Mäntele, W.; Corrie, J. E. T.; Trentham, D. R. *J. Am. Chem. Soc.* **1995**, *117*, 10 311−10 316. Barth, A.; Corrie, J. E. T.; Gradwell, M. J.; Maeda, Y.; Mäntele, W.; Meier, T.; Trentham, D. R. *J. Am. Chem. Soc.* **1997**, *119*, 4149−4159. Rammelsberg, R.; Boulas, S.; Chorongiewski, H.; Gerwert, K. *Vibr. Spectrosc.* **1999**, *19*, 143−149.
(39) Choi, J.; Terazima, M. *Photochem. Photobiol. Sci.* **2003**, *2*, 767−773.

(40) Corrie, J. E. T.; Trentham, D. R. *Bioorg. Photochem. Vol. 2*, Morrison, H., Ed., **1993**, 243−305.
(41) Peng, L.; Nachon, F.; Wirz, J.; Goeldner, M. *Angew. Chem., Int. Ed. Engl.* **1998**, *37*, 2691−2693.
(42) Schaper, K.; Dommaschke, D.; Globisch, S.; Madani-Mobarekeh, S. A. *J. Inf. Rec.* **2000**, *25*, 339−354.
(43) Walbert, S.; Pfleiderer, W.; Steiner, U. E. *Helv. Chim. Acta* **2001**, *84*, 1601−1611.

2-nitrosobenzaldehyde (**4**), which exhibits strong N=O (1501 cm^{-1}) and C=O (1700 cm^{-1}) bands, was observed on a time scale of seconds in CD$_2$Cl$_2$ (reaction **c4**, Figure 12). The release of methanol in the course of the last reaction is demonstrated by a substantial narrowing of the OH-stretch absorption (Figure 15). The pH- and buffer dependencies of reactions **ab**, **bc**, and **c4** in aqueous solution were studied in detail by optical LFP. For comparison with the TRIR measurements, LFP of **1** was also done in aprotic solvents and acetonitrile-water mixtures to establish that the same sequence of reactions occurs in protic and aprotic solvents.

A Revised Mechanism for the Light-Induced Reactions 2-Nitrobenzyl Ethers in Aqueous Solution. The neutral *aci*-tautomer of 2-nitrotoluene has a pK_a of 3.6.[8] We expected that of *aci*-**1** to be similar, because the delocalization of charge from the methoxy substituent (+M) should be largely counteracted by its inductive effect (−I). Indeed, the rate of ionization of the *aci*-transients **A**, $k_{-\text{H}} = (2.7 \pm 0.3) \times 10^6$ s^{-1}, indicated pK_a(**A**) ≈ 4. The IR-spectra of **A** show that these weak acids do not ionize in acetonitrile, suggesting p$K_a \geq 3$. In aqueous solution at physiological pH the *aci*-transients will be predominantly converted to their ionized form **A**$^-$, and the observed acid catalysis may be attributed to an increase in the equilibrium concentration of the more reactive neutral species **A**, as discussed above. Assuming a pK_a(**A**) of about 4, one would then expect acid catalysis to saturate at pH < 4. However, the decay rates of the two *aci*-nitro transients **A1** and **A2** formed from **1** do not reach a constant value at pH < 4 but increase further down to pH 2 (Figure 4), where they escape detection by nanosecond LFP. Moreover, the addition of acid also accelerated the decay rate of transients **A** in aprotic solvents, where ionization to **A**$^-$ does not occur.

We conclude that the lifetime of the aci-*intermediates is shortened by an additional, acid-catalyzed reaction.* In fact, the slope of log k_{obs} for reaction **ab2**(**1**) approaches a value of −2 between pH 4−6 in the pH-rate profile, Figure 4, indicating that two protonation steps must be involved in the decay of **A2**$^-$ in that pH region. On the other hand, an onset of saturation in acid catalysis is discernible from a short plateau at pH 4−5 in the pH-rate profile of transient **A2** formed from **2** (Figure 16), but its decay rate starts to rise again below pH 4. An acid-catalyzed reaction for transients **A** is introduced in the revised mechanism shown for **1** in Scheme 4. Here, the *aci*-nitro intermediate **A** is considered to be both an acid, p$K_{a,2} \approx 4$, and a weak base. In our previous study of parent 2-nitrotoluene[8] we have shown that protonation of *aci*-nitrotoluene leads to a *Nef*-type reaction yielding 2-nitrosobenzyl alcohol.[44] The protonated *aci*-cation **A**$^+$ of 2-nitrotoluene was found to be a strong acid, p$K_{a,1} < -3$. We may anticipate that the corresponding cation **A**$^+$ derived from **1** is substantially less acidic due to the stabilizing effect of the methoxy group. By analogy with nitrotoluene, hydration of the protonated intermediate **A**$^+$ is then assumed to yield a nitroso hydrate **B'**. The acid-catalyzed reaction via **A**$^+$ accounts for the observation of acid catalysis at pH values below p$K_{a,2}$ in aqueous solution as well as for the acceleration of the decay of neutral **A** in acetonitrile solution by acids.

---

(44) This product could not be isolated from the strongly acidic solutions, but was tentatively identified on the basis of its transient UV spectrum and the rate of dehydration of its nitroso hydrate precursor.

Scheme 4: Revised Mechanism for the Thermal Reactions of the Primary Photochemical *aci*-Transients A Formed from **1** in Aqueous Solution.^{a}
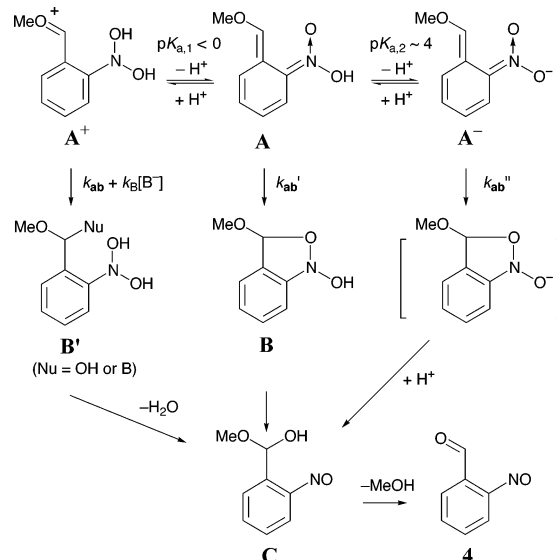
^{a} Only one isomer is shown for intermediates **A** and **B**.

To derive the rate law for the decay of intermediates **A** from Scheme 4, we assume that the acid−base equilibria between **A**$^+$, **A**, and **A**$^-$ are fully established within the lifetime of the *aci*-intermediates and that $K_{a,1} \gg$ [H$^+$] for pH ≥ 1, i.e., that **A** is quantitatively protonated only at pH values well below the range investigated. With these assumptions,[45] analysis of Scheme 4 leads to eq 4 for the pH- and buffer-dependent first-order decay rate constant k_{obs} of the *aci*-transients **A**. In the absence of buffers, [B$^-$] = 0 M, eq 4 simplifies to eq 1, which was used to fit the pH-rate profile of the *aci*-transients of **1** (Figure 4).

$$k_{\text{obs}} = \frac{k_{\text{ab}}''K_{a,2} + k_{\text{ab}}'[\text{H}^+] + (k_{\text{ab}} + k_{\text{B}}[\text{B}^-])[\text{H}^+]^2/K_{a,1}}{[\text{H}^+] + K_{a,2}}$$

(4)

Geometrical Isomerism of the Transient Intermediates A and B Formed from 1. The decay of the primary *aci*-transient **A** of **1** ($\lambda_{\text{max}} = 420$ nm) is clearly biphasic at pH > 5, in common with some other *aci*-nitro decays.[40,46,47] Below pH 5, the two decay rates nearly merge, but they become clearly separated with increasing buffer concentrations (Figure 7). Several observations show that transient **A** is a mixture of two species, **A1** and **A2**. The two rate constants obtained from the biexponential fits obeyed distinct pH-rate profiles and buffer dependencies. Moreover, the decay of the short-lived component was accompanied by a noticeable blue shift of the absorption maximum. Following a suggestion of Zhu et al.,[47b] we attribute the biphasic decay of **A** to the presence of *E*- and *Z*-isomers

---

(45) The preequilibrium assumption is not required for the protonation of **A**. As long as $K_{a,1} \gg$ [H$^+$], **A**$^+$ will always be present in low concentration, and the steady-state approximation holds for **A**$^+$. In this case the term (k_{ab} + k_{B}[B$^-$]) in eq 4 is replaced by (k_{ab} + k_{B}[B$^-$])k_{H}/(k_{ab} + k_{B}[B$^-$] + $k_{-\text{H}}$), where k_{H} and $k_{-\text{H}}$ are the rates of protonation of **A** and deprotonation of **A**$^+$, respectively. The preequilibrium assumption clearly holds for intermediates **A** and **A**$^-$ formed from **1**, because reactions **ab** are rate-limiting for the formation of **C** at pH > 6. The case of **2** will be discussed below.

(46) Peng, L.; Goeldner, M. *J. Org. Chem.* **1996**, *61*, 185−191.

(47) (a) Schupp, H.; Wong, W. K.; Schnabel, W. *J. Photochem.* **1987**, *36*, 85−97. (b) Zhu, Q. Q.; Schnabel, W.; Schupp, H. *J. Photochem.* **1987**, *39*, 317−332.
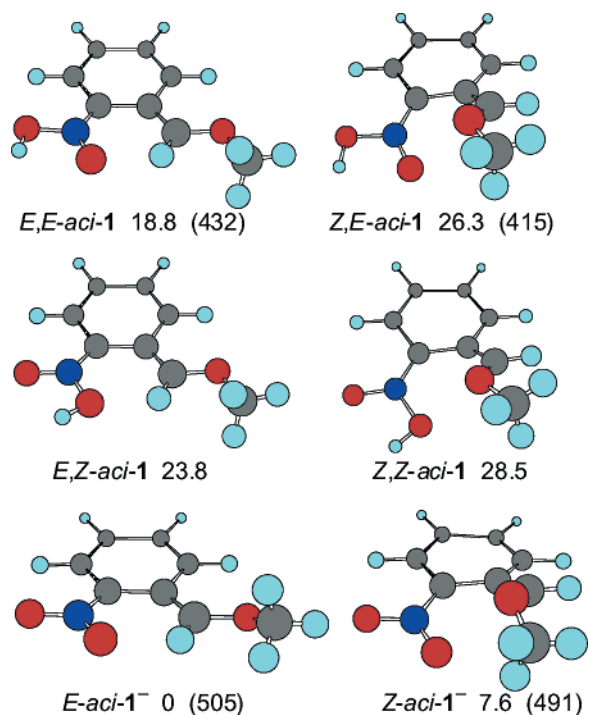
Figure 18. Calculated structures of the four *aci*-isomers of *2*-nitrobenzyl methyl ether (**1**). The energies of the nitronic acids are given in kcal mol^{-1} relative to that of the *anti*-conformer of **1** (structure shown in Figure 1), that of *Z-aci-***1**$^-$ relative to *E-aci-***1**$^-$. The wavelengths (λ/nm) of the first electronic transitions that were predicted by TD-DFT calculations are given in brackets.

with regard to the =C−OCH$_3$ group, which cyclize with different rates.

The calculated geometries of the four isomeric *aci*-tautomers of **1** and their energies relative to that of **1** are shown in Figure 18. Least-motion hydrogen transfer from the benzylic carbon of **1** to the nitro group would form the *E,Z*- and *Z,Z*-isomers as the primary photoproducts. The calculations indicate that the *E,E*- and *Z,E*-isomers, in which the OH group of the nitronic acid is situated trans, are several kcal mol^{-1} lower in energy. We may assume that the equilibrium between the two protonation sites on the nitronic acid function is established on the ns time scale in aqueous solution. Ionization of *aci*-**1** occurs with a rate constant of 2.7×10^6 s^{-1} in water, and is accelerated in the presence of buffers or base. Moreover, separation of the ion pair formed upon protonation of water is not required for proton transfer between the O atoms of the nitronic acid function. A hydrogen-bonded water molecule may act as a proton shuttle through a six-membered ring. Indeed, the calculated barrier for intramolecular *E* to *Z* isomerization in the *aci*-tautomer of nitrotoluene was 20.3 kcal mol^{-1} in the gas phase, but was lowered to 10.1 kcal mol^{-1} in the presence of one water molecule.[36] In the following discussion we will, therefore, assume that *only geometrical isomerism at the exocyclic C=C double bond, designated by the first label* E *or* Z, *gives rise to kinetically distinguishable* aci-*transients in aqueous solution.*

Steric congestion in the isomers with *Z*-configuration at the methylene group is apparent from both the structures and the relative energies given in Figure 18. The blue shift of the absorption maximum associated with the decay of the short-lived component **A1**$^-$ suggests that its exocyclic groups are twisted at the double bond.[48] However, TD-DFT calculations
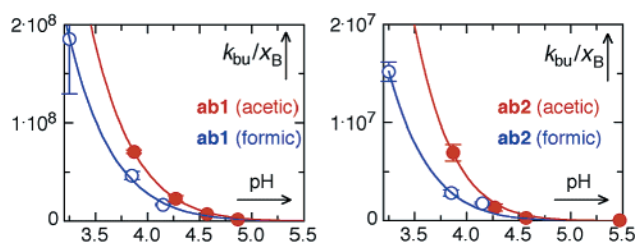
Figure 19. Buffer slopes k_{bu} (Table 2) obtained for transients **A1** (left) and **A2** (right) formed from **1** in acetic (●, red) and formic (○, blue) acid buffers plotted as a function of buffer pH. The solid lines were obtained by nonlinear least-squares fitting of eq 5.

do not support this, predicting longer wavelengths of absorption for the *E*-isomers (Figure 18). Also, one would expect the twisted *Z*-isomer to be the more reactive. However, SCRF calculations in water predicted a smaller barrier for the cyclization of *E,E-aci-***1** (8.4 kcal/mol) than of *Z,E-aci-***1** (10.3 kcal/mol).[36] In view of these rather conflicting indications, we refrain from attempting an assignment of transients **A1** and **A2** to the structural isomers.

Catalysis by Buffers. Protonation Equilibria of Transients A Formed from 1 in Aqueous Solution. Unambiguous evidence for the occurrence of an acid-catalyzed path involving protonation of **A** to **A**$^+$ comes from the observation of *general* acid catalysis on the decay of **A** (Table 2). Buffer catalysis affecting reactions **ab1** and **ab2** must be due to the acidic buffer component, because the decay of **A** is not accelerated by hydroxyl ions, the strongest possible base in aqueous solution. Rapid equilibration of **A**$^-$ with **A**, followed by rate-determining cyclization of **A** to **B**, would give rise to *specific* acid catalysis on the decay of **A**$^-$, because the general acid does not participate in the rate-determining cyclization step **A** → **B**.

The additional reaction path via **A**$^+$ introduced in Scheme 4 accounts for the effect of buffers on the decay rate of the *aci*-transients. Protonation of **A** might be the rate-determining step followed by rapid hydrolysis to **B′** (Nu = OH). This would give rise to general acid catalysis, but is considered unlikely, because even protonation of the weaker base *aci*-nitrotoluene is reversible.[8] Alternatively, the cation **A**$^+$ may be trapped preferentially by the basic buffer component B$^-$ to give **B′** (Nu = B). The combination of preequilibrium protonation (specific acid catalysis) with a rate-determining general-base-catalyzed step results in apparent general acid catalysis.

Three buffer systems were studied at various buffer ratios, namely formic acid/sodium formate, acetic acid/sodium acetate, and potassium dihydrogen phosphate/disodium monohydrogen phosphate. The slopes k_{bu}, obtained from the buffer dilution plots (e.g., Figure 7), correspond to the derivative of eq 4 with respect to the total buffer concentration, [bu] = [HB] + [B$^-$]. Making use of the relation [B$^-$] = x_B[bu], where x_B = [B$^-$]/([HB] + [B$^-$]), we obtain eq 5.

$$k_{bu} = \left(\frac{\partial k_{obs}}{\partial [bu]}\right)_{[H^+]} = x_B \left(\frac{\partial k_{obs}}{\partial [B^-]}\right)_{[H^+]} = \frac{x_B k_B [H^+]^2}{K_{a,1}(K_{a,2} + [H^+])} \quad (5)$$

Plots of the dependence of k_{bu}/x_B on pH in acetic and formic acid buffers are shown in Figure 19.

(48) Quinkert, G. Wiersdorff, W.-W. Finke, M.; Opitz, K. von der Haar, F.-G. *Chem. Ber.* **1968**, *101*, 2302−2325.
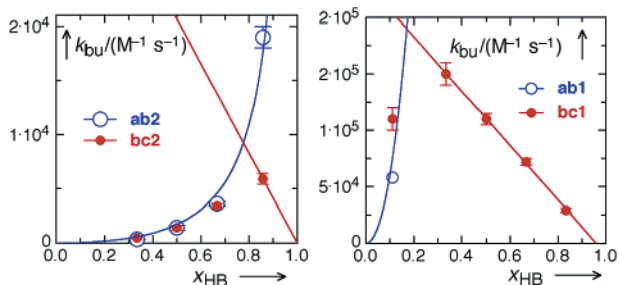
Figure 20. Buffer slopes k_{bu} (Table 2) obtained for reactions **ab2** (○) and **bc2** (●) in phosphate buffers (left-hand figure) and **ab1** (○) and **bc1** (●) in acetic acid buffers (right-hand figure) plotted as a function of buffer composition x_{HB}. The curved lines for reactions **ab** were obtained by nonlinear least-squares fitting of eq 5 to the buffer slopes for reactions **ab**. To express eq 5 as a function of the variable x_{HB} only, [H$^+$] was replaced by $K_a^{bu}x_{HB}/(1 - x_{HB})$. The red straight lines indicate the x_{HB}-dependence for reactions **bc** that would be expected in the absence of the rate-limitation by reactions **ab**.

Equation 5 simplifies to $k_{bu} \approx x_B k_B [\text{H}^+]/K_{a,1}$ for $[\text{H}^+] \gg K_{a,2}$, and to $k_{bu} \approx x_B k_B [\text{H}^+]^2/(K_{a,1}K_{a,2})$ for $[\text{H}^+] \ll K_{a,2}$. Thus, in plots of $\log(k_{bu}/x_B)$ versus pH, the slope should change from -2 to -1 in buffer systems with pH $\approx$ p$K_{a,2}$. That was found to be the case and provided the most reliable estimates of p$K_{a,2}$. The values obtained for reaction **ab2** were -2.23 ± 0.07 (phosphate buffers, pH 6–7),[49] -1.63 ± 0.15 (acetate buffers, pH 4–5), and -1.14 ± 0.12 (formate buffers, pH 3–4). The p$K_{a,2}$ of **A2** must, therefore, be close to 4.5. The p$K_{a,2}$ of **A2** so obtained agrees well with that estimated from the negative curvature around pH 4.5 in the pH-rate profile of reaction **ab2** (Figure 4). Similarly, reaction **ab1** gave slopes for $\log(k_{bu}/x_B)$ versus pH of -1.96 ± 0.12 for acetate and -1.00 ± 0.08 for formate (the value in phosphate buffers was not defined accurately for reaction **ab1**), which indicates that the p$K_{a,2}$ of **A1** is about 4.0.

Acid and Base Catalysis of bc1 and bc2. Reactions **bc1** and **bc2** also exhibited buffer catalysis. In contrast to the rather exceptional buffer dependence discussed above (eq 5), plots of buffer catalytic coefficients, k_{bu}, versus the molar fraction of the acidic buffer component, $x_{HB} = [\text{HB}]/([\text{HB}] + [\text{B}^-])$, are commonly linear, eq 6. This allows separation of k_{bu} into its general acid, k_{HB} ($x_{HB} = 1$), and general base, k_B ($x_{HB} = 0$), components.

$$k_{bu} = k_B + (k_{HB} - k_B) x_{HB} \qquad (6)$$

Plots of the buffer coefficients obtained in acetic acid buffers (Table 2) were indeed linear in most cases, and indicated that catalysis is due to the basic buffer component, $k_B(\textbf{bc1}) = (2.3 \pm 0.5) \times 10^5$ M^{-1} s^{-1} and $k_B(\textbf{bc2}) = (5.5 \pm 0.4) \times 10^2$ M^{-1} s^{-1}. The intercepts at $x_{HB} = 1$ were not significantly different from zero. The buffer slopes k_{bu} for reaction **bc2** in phosphate buffers (Figure 20, left) and for reaction **bc1** in acetate buffers (right) changed in a strongly nonlinear fashion with x_{HB}. These anomalies arise from a change in the rate-limiting step of the reactions. As can be seen from the pH-rate profile, Figure 4, reactions **bc** limit the rate of formation of **C** at pH $\ll$ 6, but reactions **ab** become rate-limiting at pH $\gg$ 6. Thus, in the basic phosphate buffer compositions, $x_{HB} < 0.5$, the rate-limiting step for the slower component in the formation of **C** is reaction **ab2**,

which is not catalyzed by general base and only weakly by the weak general acid H$_2$PO$_4^-$. As we move to more acidic buffer compositions, reaction **ab2** becomes faster than **bc2**, and the latter now limits the rate of formation of **C**. The acceleration of reaction **bc2** by the buffer at $x_{HB} = 0.85$ may be attributed to the remaining fraction of the general base HPO$_4^{2-}$. Similarly, the rate of reaction **bc1** increases linearly in the acetate buffers down to $x_{HB} = 0.3$, but then suddenly drops, because reaction **ab1** becomes rate-limiting.

pH-Rate Profiles of Transients A–C Formed from 1 in Aqueous Solution (Figure 4). Inspection of Figure 4 reveals the sequence of reactions from the primary *aci*-nitro transients **A** to the final product 2-nitrosobenzaldehyde (**4**) and methanol in aqueous solutions of various pH. The release of methanol coincides with decay of the two isomeric *aci*-nitro transients only at pH values > 9. Calculations[22,36] suggest that the reactions of the *aci*-anions **A1**$^-$ and **A2**$^-$ proceed directly to the hemiacetal **C**; the anions of the cyclic intermediates **B** were found not to be stable intermediates. The hemiacetals **C** rapidly eliminate methoxide in basic solutions.

Carbon protonation of **A**$^-$ by water to regenerate **1** is too slow to compete with the formation of **C**. That reaction, which was observed for the *aci*-tautomer of 2-nitrotoluene in basic aqueous solutions, exhibits a large kinetic isotope effect, $k_{ab}^H/k_{ab}^D = 7.2$.[8] The kinetic isotope effects for the decay of **A1**$^-$ and **A2**$^-$, on the other hand, are unity within experimental error. The decay of the hemiacetal **C** (compound **7**) is the rate-determining step for the release of methanol at pH < 8. At pH values in the range of 3–6 its lifetime reaches nearly 1 min and is 5–8 orders of magnitude longer than those of the primary *aci*-intermediates **A**.

The cyclic intermediates **B** (compound **6**) are observable only at pH < 6 in water and in aprotic solvents. At pH > 6 they decay more rapidly than they are formed. Assignment of reaction **bc** to ring-opening of the cyclic intermediates **6** to the 2-nitrosohemiacetal **7** is based on the TRIR measurements. Why do we observe biexponential kinetics for reaction **bc**? The inversion barriers of amines increase strongly upon electronegative substitution.[50] Amines carrying two oxygen atoms reach inversion barriers of up to 30 kcal mol^{-1}.[51] The nitrogen inversion barriers for a number of isoxazolidine derivatives were found to be in the range of 14–16 kcal mol^{-1},[52a] that in 1-hydroxy-2,2,4,4-tetramethylpyrrolidine is 12 kcal mol^{-1}.[52b] DFT calculations for the inversion barrier in **6** gave 16.8 kcal mol^{-1} (Figure 21).[36] Apparently, the flattening effect of the conjugated aromatic ring in **6** is overcompensated by substitution with a second oxygen atom on nitrogen. Thus, we may assume that equilibration between the two stereoisomers of **6** is slow compared to ring opening to the hemiacetal **7**.

Ring opening of **B** might be concerted with elimination of CH$_3$OH yielding the aldehyde **4** directly. For aprotic solvents this is ruled out by the results of the TRIR-measurements. The intermediate **C** formed from **B** does not carry a carbonyl group. In aqueous solutions the final reaction **c4** was monitored by its UV-spectral changes (Figure 6). The initial spectrum recorded a few seconds after photolysis corresponds to that expected for

(49) The value somewhat below -2 may be due to a contribution of catalysis by H$_3$PO$_4$ in this buffer system. Loudon, G. M.; Ryono, D. E. *J. Org. Chem.* **1975**, *40*, 3574–3577.

(50) Lehn, J. M. *Top. Curr. Chem.* **1970**, *15*, 311–377.
(51) Müller, K.; Eschenmoser, A. *Helv. Chim. Acta* **1969**, *52*, 1823–1830.
(52) (a) Hassan, A.; Wazeer, M. I. M.; Perzanowski, H. P.; Ali, S. A. *J. Chem. Soc., Perkin Trans. 2* **1997**, 411–418. (b) Perrin, C. L.; Thoburn, J. D.; Elsheimer, S. *J. Org. Chem.* **1991**, *56*, 7034–7038.
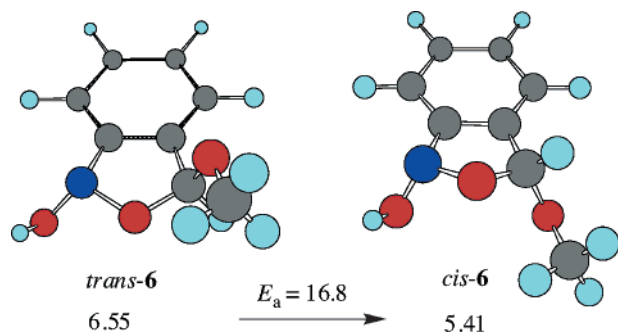
Figure 21. Geometries and energies (kcal mol^{-1}) of intermediates **B** = **6**.

the hemiacetal C (7), which has a lifetime of nearly one min and limits the release rate of methanol from 1 in aqueous solutions of pH < 8. There is no indication for a direct decay path of B to 4.

Scheme 4 introduces an acid-catalyzed path affording nitroso hydrates **B′** via the protonated *aci*-nitro intermediates **A$^+$** in strongly acidic and in buffered solutions. We cannot distinguish between intermediates **B** and **B′** (Nu = OH or B) by optical LFP. Thus, the rate constants determined for reaction **bc** at pH < 5 should probably be attributed to dehydration of **B′** yielding the hemiacetal **C**. The rate constants k_H determined for these reactions agree well with those reported for related nitroso hydrates.[53]

The pH-rate profile of reaction **c4** shown in Figure 4 exhibits acid and base catalysis. In buffer solutions both general acid and general base catalysis were observed. The corresponding buffer slopes (Table 2) are comparable to those determined for the decay of the methyl- and ethyl hemiacetals of benzaldehyde.[54,55] Therefore, the release of methanol can be accelerated slightly by the addition of buffers. The final product 2-nitrosobenzaldehyde (**4**) is sensitive to light as well as to acid and base. In aqueous solution at room temperature, the coefficients for acid and base-catalyzed decomposition are $k_H \approx 20$ M^{-1} s^{-1} and $k_{OH} \approx 5 \times 10^5$ M^{-1} s^{-1}, respectively. Product **4** is no longer detectable at pH > 9, where its decay rate exceeds that of its formation from **1**.

pH-rate Profiles of Transients A−C Formed from 2 and 3 (Figures 16 and 17). The pH-rate profiles obtained for **2** show many similarities with those of **1**, but a qualitative difference should be noted: The rate constant of the fast component **A1** is independent of pH. Scheme 4 (adapted to **2** by adding a methyl group to the structures) accounts for this change, if we drop the preequilibrium assumption for the faster-decaying transient **A1**. If cyclization of the primary photoproduct **A1** is faster than ionization to **A1$^-$**, then we expect to see a biexponential decay of **A**, because the transient absorption by **A1** disappears to the transparent product **B1**, while **A2** ionizes to the longer-lived anion **A2$^-$**, which still absorbs at 420 nm.

Calculations and several observations strongly support the hypothesis that *cyclization of intermediate A1 competes effectively with ionization to A1$^-$*. (*i*) DFT calculations[36] have shown that the barrier of cyclization **A → B** is strongly reduced

(53) Grünbein, W.; Fojtik, A.; Henglein, A. *Monatsh. Chem.* **1970**, *101*, 1243−1252.
(54) Capon, B.; Nimmo, K.; Reid, G. L. *J. Chem. Soc., Chem. Commun.* **1976**, 871−873.
(55) McClelland, R. A.; Kangasabapathy, V. M.; Mathivanan, N. *Can. J. Chem.* **1991**, *69*, 2084−2093.

by α-substituents, from 20 kcal mol^{-1} for the *aci*-tautomer of nitrotoluene, to 14 kcal mol^{-1} for that of 2-nitrophenethyl, and to 8 kcal mol^{-1} for that of **1**. We have performed the same calculations for the *E,E*- and *E,Z-aci*-isomers of **2**, which gave 5 kcal mol^{-1} for the more reactive *E,E*-isomer in water. This low barrier, combined with an Arrhenius preexponential factor of $A = 10^{13}$ s^{-1} provides an estimate of the rate of cyclization, $k_{ab}' \approx 10^7$ s^{-1}, which is comparable to the rate of ionization, $k_{-H} \approx 10^7$ s^{-1}. The fit of eq 1 to the observed rate constants gives $k_{ab}' = 5.2 \times 10^7$ s^{-1} for transient **A1** formed from **2**, but much smaller values, $k_{ab}' = 8.7 \times 10^5$ and 1.4×10^4 s^{-1}, for transients for **A1** and **A2**, respectively, formed from **1**. (*ii*) The formation of **C(2)** is biphasic at pH > 8. The rate of the slow wave is limited by the decay of **A2$^-$**, but that of the fast, major wave continues to rise linearly with increasing base concentration until it vanishes at pH 12 (Figure 17). This proves that the major part of intermediate **B** is formed directly from nascent **A1** by the fast, pH-independent reaction. (*iii*) Deprotonation of **A1** is accelerated by hydroxyl ions in aqueous base, $k_{OH} \sim 1 \times 10^{10}$ M^{-1} s^{-1}, and this will diminish the amount of **B** formed by the fast reaction. Deprotonation of **A1** to **A1$^-$** by hydroxyl ions becomes faster than cyclization, $k_{ab}'(A1) = 5.2 \times 10^7$ s^{-1}, at about pH 12.5. Consistently, the fast wave in the formation of **C** was still detectable at pH 12, but vanished, leaving only the slow wave, at pH 13.

The pH-rate profile obtained by LFP of caged ATP (**3**) is shown in Figure 17. First we note, in agreement with previous work,[32] that the decay of *aci*-**3** obeys a first-order rate law accurately. The bulky ATP substituent may favor formation of a single *aci*-isomer in the primary photoreaction, or the occurrence of a fast wave, as in **2**, may have escaped observation. Otherwise, the analogy to the behavior of the *aci*-transients **A** formed from **1** and **2** is evident. The decay rates increase from pH 10 down to pH 2, where they exceed the time resolution of nanosecond LFP. *At pH > 6, the appearance rate of product 5 matches the decay rate of the aci-nitro tautomer A, as established by Walker et al.[32] However, for pH < 6 the decay rate of A exceeds the rate of formation of 5, requiring an additional intermediate B, which does not absorb above 300 nm.* Intermediate **B** does not delay the release of ATP at physiological pH values, because triphosphate is a much better leaving group than methoxide in **1** or **2**. The decay of **B** could, however, become rate-limiting in different media.

Comparison with a Related Study of Derivatives of 1 and 2. A study of several derivatives of **1** and **2**, in particular the glycolic acid ethers **8** and **9**, by fast-scan FTIR and LFP was published recently by Corrie et al.[6] Their experimental data for **8** and **9** are largely in agreement with our results on **2** and **1**, respectively, inasmuch as the conditions of measurement are comparable. It should be noted that the IR-spectrum reported by Corrie et al. (Figure 3)[6] for the *aci*-nitro intermediate formed from **9** bears no relation to that of transient **A** determined here (Figure 10). Their spectrum was obtained in aqueous solution at pH 8.5. It is, therefore, the spectrum of the ionized *aci*-anion **A$^-$**. Our spectrum was recorded in acetonitrile, where **A** does not ionize. Surprisingly, Corrie et al. report first-order decay rates for the *aci*-nitro transient formed from **9**, while that from **1** exhibits dual exponential decay as shown here and elsewhere.[40,56]

(56) Corrie, J. E. T. *J. Chem. Soc., Perkin Trans. 1* **1993**, 2161−2166.

8   R = Me
9   R = H
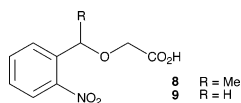
We concur with two important conclusions drawn by Corrie et al.[6] from their study of compounds **8** and **9**. First, the intermediate **C** formed from the nitrophenethyl ethers **2** and **8** is a hemiketal that is much longer-lived than the readily observable *aci*-intermediates **A**, and determines the rate of alcohol release under physiological conditions (pH ≈ 7). Second, at pH > 7 the formation of the hemiketal **C** from **2** and **8** takes place in two waves of substantially different rates, whereas only a single wave is found with the nitrobenzyl ethers **1** and **9**.

However, we disagree on essential points regarding the reaction mechanism: (1) Corrie et al. claimed that the fast formation of **C** from **8** proceeds directly from **A**, bypassing the cyclic intermediate **B** ("two-path mechanism"). To explain some difficulties with this hypothesis, they had to invoke reaction from a vibrationally excited state of **A**. We have identified the short-lived precursor **A1** formed from **2** with a lifetime of about 20 ns, which is much too long for a vibrationally excited molecule, and have shown that it does react via a cyclic intermediate **B1**. (2) Buffer catalysis accelerating the decay of the ionized *aci*-anions **A⁻**, which was noted by Corrie et al. and defined here as general acid catalysis, is not consistent with any of the previously proposed mechanisms. An additional, general-acid catalyzed reaction must be operating. (3) Corrie et al. explicitly excluded reaction of **9** via a hemiacetal **C**, and concluded that the cyclic intermediate **B** in this case decays directly to the end product 2-nitrosobenzaldehyde (**4**). However, intermediate **B** formed from **1** does react via a long-lived hemiacetal **C**, which limits the release rate of methanol in aqueous solution up to pH 8.[57] The IR spectra of the hemiketal intermediates reported by Corrie et al.[6] exhibit much the same prominent features (absence of a carbonyl band, nitroso band

at 1497 cm^{-1}, bands around 1100−1200 and 1420 cm^{-1}) as that of the hemiacetal intermediate **C** formed from **1** (Figure 14). We surmise that the failure of Corrie et al. to detect the hemiacetal formed from **9** may be attributed to their reaction conditions: At pH 8.5 intermediate **C** decays more rapidly than it is formed (Figure 4). We maintain that the findings of Corrie et al. as well as our more extensive observations are fully compatible with the single mechanistic Scheme 4 presented above.

Conclusion. Photorelease of methanol from 2-nitrobenzyl and 2-nitrophenethyl methyl ethers (**1** and **2**) in wholly aqueous solutions and in organic solvents proceeds via three intermediates, the primary *aci*-nitro transients **A** ($\lambda_{max} \approx 400$ nm), the 1,3-dihydrobenz[*c*]isoxazol-1-ol derivatives **B** observed here for the first time, and 2-nitrosobenzyl hemiacetals **C**. A general-acid-catalyzed reaction, which proceeds via nitroso hydrates **B′**, prevails in buffered aqueous solutions. This process was not previously taken into account. At pH values above 10, where the lifetime of transients **A⁻** becomes independent of pH, the release of methanol occurs in a single step. The decay of intermediate **C** limits the release rate of methanol up to pH 8 and 10 for **1** and **2**, respectively. An intermediate of type **B** limits the release rate of ATP from 'caged ATP' (**3**) at pH values ≤ 6. The rates of the reaction paths shown in Scheme 4 may vary strongly with the nature of the reaction medium (solvent, pH, and buffer concentration) and of the leaving group. The lifetimes of the secondary intermediates **B** or **B′** and **C** may exceed that of the primary *aci*-nitro transients **A** by orders of magnitude. Therefore, the easily observable decay rates of transients **A** are not, in general, a good indicator for the release rate of the leaving group.

Supporting Information Available: Rate data for the pH-rate profiles and the buffer dilution plots. Details of quantum chemical calculations. This material is available free of charge via the Internet at http://pubs.acs.org.

JA039071Z

(57) Observation of a long-lived hemiacetal intermediate formed by photolysis of a 2-nitrobenzyl ether has been reported previously: Hirayama, Y.; Iwamura, M.; Furuta, T. *Bioorg. Med. Chem. Lett.* **2003**, *13*, 905−908. See also: Peyser, J. R.; Flechtner, T. W. *J. Org. Chem.* **1987**, *52*, 4645−4646.